



HAL
open science

Disentangling weak and strong interactions in $B \rightarrow K^*(\rightarrow K\pi)\pi$ Dalitz-plot analyses

Jérôme Charles, Sébastien Descotes-Genon, José Ocariz, Alejandro Pérez
Pérez

► **To cite this version:**

Jérôme Charles, Sébastien Descotes-Genon, José Ocariz, Alejandro Pérez Pérez. Disentangling weak and strong interactions in $B \rightarrow K^*(\rightarrow K\pi)\pi$ Dalitz-plot analyses. *European Physical Journal C: Particles and Fields*, 2017, 77 (8), pp.561. 10.1140/epjc/s10052-017-5133-x . hal-01581150

HAL Id: hal-01581150

<https://hal.sorbonne-universite.fr/hal-01581150>

Submitted on 4 Sep 2017

HAL is a multi-disciplinary open access archive for the deposit and dissemination of scientific research documents, whether they are published or not. The documents may come from teaching and research institutions in France or abroad, or from public or private research centers.

L'archive ouverte pluridisciplinaire **HAL**, est destinée au dépôt et à la diffusion de documents scientifiques de niveau recherche, publiés ou non, émanant des établissements d'enseignement et de recherche français ou étrangers, des laboratoires publics ou privés.



Distributed under a Creative Commons Attribution 4.0 International License

Disentangling weak and strong interactions in $B \rightarrow K^*(\rightarrow K\pi)\pi$ Dalitz-plot analyses

Jérôme Charles¹, Sébastien Descotes-Genon^{2,a}, José Ocariz^{3,4}, Alejandro Pérez Pérez⁵, For the CKMfitter Group

¹ CNRS, Aix-Marseille Univ, Université de Toulon, CPT UMR 7332, 13288 Marseille Cedex 9, France

² Laboratoire de Physique Théorique (UMR 8627), CNRS, Univ. Paris-Sud, Université Paris-Saclay, 91405 Orsay Cedex, France

³ Sorbonne Universités, UPMC Univ. Paris 06, UMR 7585, LPNHE, 75005 Paris, France

⁴ Université Paris Diderot, LPNHE UMR 7585, Sorbonne Paris Cité, 75252 Paris, France

⁵ Université de Strasbourg, CNRS, IPHC UMR 7178, 67000 Strasbourg, France

Received: 15 April 2017 / Accepted: 6 August 2017

© The Author(s) 2017. This article is an open access publication

Abstract Dalitz-plot analyses of $B \rightarrow K\pi\pi$ decays provide direct access to decay amplitudes, and thereby weak and strong phases can be disentangled by resolving the interference patterns in phase space between intermediate resonant states. A phenomenological isospin analysis of $B \rightarrow K^*(\rightarrow K\pi)\pi$ decay amplitudes is presented exploiting available amplitude analyses performed at the BABAR, Belle and LHCb experiments. A first application consists in constraining the CKM parameters thanks to an external hadronic input. A method, proposed some time ago by two different groups and relying on a bound on the electroweak penguin contribution, is shown to lack the desired robustness and accuracy, and we propose a more alluring alternative using a bound on the annihilation contribution. A second application consists in extracting information on hadronic amplitudes assuming the values of the CKM parameters from a global fit to quark flavour data. The current data yields several solutions, which do not fully support the hierarchy of hadronic amplitudes usually expected from theoretical arguments (colour suppression, suppression of electroweak penguins), as illustrated from computations within QCD factorisation. Some prospects concerning the impact of future measurements at LHCb and Belle II are also presented. Results are obtained with the CKMfitter analysis package, featuring the frequentist statistical approach and using the Rfit scheme to handle theoretical uncertainties.

1 Introduction

Non-leptonic B decays have been extensively studied at the B -factories BABAR and Belle [1], as well at the LHCb experiment [2]. Within the Standard Model (SM) some of

these modes provide valuable information on the Cabibbo–Kobayashi–Maskawa (CKM) matrix and the structure of CP violation [3,4], entangled with hadronic amplitudes describing processes either at the tree level or the loop level (the so-called penguin contributions). Depending on the transition considered, one may or may not get rid of hadronic contributions which are notoriously difficult to assess. For instance, in $b \rightarrow c\bar{c}s$ processes, the CKM phase in the dominant tree amplitude is the same as that of the Cabibbo-suppressed penguin one, so the only relevant weak phase is the B_d -mixing phase 2β (up to a very high accuracy) and it can be extracted from a CP asymmetry out of which QCD contributions drop to a very high accuracy. For charmless B decays, the two leading amplitudes often carry different CKM and strong phases, and thus the extraction of CKM couplings can be more challenging. In some cases, for instance the determination of α from $B \rightarrow \pi\pi$ [5], one can use flavour symmetries such as isospin in order to extract all hadronic contributions from experimental measurements, while constraining CKM parameters. This has provided many useful constraints for the global analysis of the CKM matrix within the Standard Model and the accurate determination of its parameters [6–9], as well as inputs for some models of New Physics [10–13].

The constraints obtained from some of the non-leptonic two-body B decays can be contrasted with the unclear situation of the theoretical computations for these processes. Several methods (QCD factorisation [14–17], perturbative QCD approach [18–23], Soft-collinear effective theory [24–28]) were devised more than a decade ago to compute hadronic contributions for non-leptonic decays. However, some of their aspects remain debated at the conceptual level [29–37], and they struggle to reproduce some data on B decays into two mesons, especially $\pi^0\pi^0$, $\rho^0\rho^0$, $K\pi$, ϕK^* , ρK^* [37]. Considering the progress performed meanwhile in the deter-

^ae-mail: descotes@th.u-psud.fr

mination of the CKM matrix, it is clear that, by now, most of these non-leptonic modes provide more a test of our understanding of hadronic process rather than competitive constraints on the values of the CKM parameters, even though it can be interesting to consider them from one point of view or the other.

Our analysis is focused on the study of $B \rightarrow K^*(\rightarrow K\pi)\pi$ decay amplitudes, with the help of isospin symmetry. Among the various $b \rightarrow u\bar{u}s$ processes, the choice of $B \rightarrow K^*\pi$ system is motivated by the fact that an amplitude (Dalitz-plot) analysis of the three-body final state $K\pi\pi$ provides access to several interference phases among different intermediate $K^*\pi$ states. The information provided by these physical observables highlights the potential of the $B \rightarrow K^*\pi$ system (VP) compared with $B \rightarrow K\pi$ (PP) where only branching ratios and CP asymmetries are accessible. Similarly, the $B \rightarrow K^*\pi$ system leads to the final $K\pi\pi$ state with a richer pattern of interferences and thus a larger set of observables than other pseudo-scalar–vector states, like, say, $B \rightarrow K\rho$ (indeed, $K\pi\pi$ exhibits K^* resonances from either of the two combinations of $K\pi$ pairs, whereas the ρ meson comes from the only $\pi\pi$ pair available). In addition, the study of these modes provides experimental information on the dynamics of pseudo-scalar–vector modes, which is less known and more challenging from the theoretical point of view. Finally, this system has been studied extensively at the BABAR [38–41] and Belle [43,44] experiments, and a large set of observables is readily available.

Let us mention that other approaches, going beyond isospin symmetry, have been proposed to study this system. For instance, one can use SU(3) symmetry and SU(3)-related channels in addition to the ones that we consider in this paper [45,46]. Another proposal is the construction of the fully SU(3)-symmetric amplitude [47] to which the spin-one intermediate resonances that we consider here do not contribute.

The rest of this article is organised in the following way. In Sect. 2, we discuss the observables provided by the analysis of the $K\pi\pi$ Dalitz-plot analysis. In Sect. 3, we recall how isospin symmetry is used to reduce the set of hadronic amplitudes and their connection with diagram topologies. In Sect. 4, we discuss two methods to exploit these decays in order to extract information on the CKM matrix, making some assumptions about the size of specific contributions (either electroweak penguins or annihilation). In Sect. 5, we take the opposite point of view. Taking into account our current knowledge of the CKM matrix from global analysis, we set constraints on the hadronic amplitudes used to describe these decays, and we make a brief comparison with theoretical estimates based on QCD factorisation. In Sect. 6, we perform a brief prospective study, determining how the improved measurements expected from LHCb and Belle II may modify the determination of the hadronic amplitudes before concluding.

In the appendices, we discuss various technical aspects concerning the inputs and the fits presented in the paper.

2 Dalitz-plot amplitudes

Charmless hadronic B decays are a particularly rich source of experimental information [1,2]. For B decays into three light mesons (pions and kaons), the kinematics of the three-body final state can be completely determined experimentally, thus allowing for a complete characterisation of the Dalitz-plot (DP) phase space. In addition to quasi-two-body event-counting observables, the interference phases between pairs of resonances can also be accessed, and CP-odd (weak) phases can be disentangled from CP-even (strong) ones. Let us, however, stress that the extraction of the experimental information relies heavily on the so-called isobar approximation, widely used in experimental analyses because of its simplicity, and in spite of its known shortcomings [48].

The $B \rightarrow K\pi\pi$ system is particularly interesting, as the decay amplitudes from intermediate $B \rightarrow PV$ resonances ($K^*(892)$ and $\rho(770)$) receive sizeable contributions from both tree-level and loop diagrams, and they interfere directly in the common phase-space regions (namely the “corners” of the DP). The presence of additional resonant intermediate states further constrain the interference patterns and help resolving potential phase ambiguities. In the case of $B^0 \rightarrow K^+\pi^-\pi^0$ and $B^+ \rightarrow K_S^0\pi^+\pi^0$, two different $K^*(892)$ states contribute to the decay amplitude, and their interference phases can be directly measured. For $B^0 \rightarrow K_S^0\pi^+\pi^-$, the time-dependent evolution of the decay amplitudes for B^0 and \bar{B}^0 provides (indirect) access to the relative phase between the $B^0 \rightarrow K^{*+}\pi^-$ and $\bar{B}^0 \rightarrow K^{*-}\pi^+$ amplitudes.

In the isobar approximation [48], the total decay amplitude for a given mode is a sum of intermediate resonant contributions, and each of these is a complex function of phase space: $\mathcal{A}(\text{DP}) = \sum_i A_i F_i(\text{DP})$, where the sum rolls over all the intermediate resonances providing sizeable contributions, the F_i functions are the “lineshapes” of each resonance, and the isobar parameters A_i are complex coefficients indicating the strength of each intermediate amplitude. The corresponding relation is $\bar{\mathcal{A}}(\text{DP}) = \sum_i \bar{A}_i \bar{F}_i(\text{DP})$ for CP-conjugate amplitudes.

Any convention-independent function of isobar parameters is a physical observable. For instance, for a given resonance i , its direct CP asymmetry A_{CP}^i is expressed as

$$A_{\text{CP}}^i = \frac{|\bar{A}_i|^2 - |A_i|^2}{|\bar{A}_i|^2 + |A_i|^2}, \quad (1)$$

and its partial fit fraction FF^i is

$$FF^i = \frac{(|A_i|^2 + |\bar{A}_i|^2) \int_{DP} |F_i(DP)|^2 d(DP)}{\sum_{jk} (A_j A_k^* + \bar{A}_j \bar{A}_k^*) \int_{DP} F_j(DP) F_k^*(DP) d(DP)}. \tag{2}$$

To obtain the partial branching fraction \mathcal{B}^i , the fit fraction has to be multiplied by the total branching fraction of the final state (e.g., $B^0 \rightarrow K_S^0 \pi^+ \pi^-$),

$$\mathcal{B}^i = FF^i \times \mathcal{B}_{\text{incl}}. \tag{3}$$

A phase difference φ_{ij} between two resonances i and j contributing to the same total decay amplitude (i.e., between resonances in the same DP) is

$$\varphi^{ij} = \arg(A_i/A_j), \quad \bar{\varphi}_{ij} = \arg(\bar{A}_i/\bar{A}_j), \tag{4}$$

and a phase difference between the two CP-conjugate amplitudes for resonance i is

$$\Delta\varphi^i = \arg\left(\frac{q \bar{A}_i}{p A_i}\right), \tag{5}$$

where q/p is the $B^0 - \bar{B}^0$ oscillation parameter.

For $B \rightarrow K^* \pi$ modes, there are in total 13 physical observables. These can be classified as four branching fractions, four direct CP asymmetries and five phase differences:

- The CP-averaged $\mathcal{B}^{+-} = \text{BR}(B^0 \rightarrow K^{*+} \pi^-)$ branching fraction and its corresponding CP asymmetry A_{CP}^{+-} . These observables can be measured independently in the $B^0 \rightarrow K_S^0 \pi^+ \pi^-$ and $B^0 \rightarrow K^+ \pi^- \pi^0$ Dalitz planes.
- The CP-averaged $\mathcal{B}^{00} = \text{BR}(B^0 \rightarrow K^{*0} \pi^0)$ branching fraction and its corresponding CP asymmetry A_{CP}^{00} . These observables can be accessed both in the $B^0 \rightarrow K^+ \pi^- \pi^0$ and $B^0 \rightarrow K_S^0 \pi^0 \pi^0$ Dalitz planes.
- The CP-averaged $\mathcal{B}^{+0} = \text{BR}(B^+ \rightarrow K^{*+} \pi^0)$ branching fraction and its corresponding CP asymmetry A_{CP}^{+0} . These observables can be measured both in the $B^+ \rightarrow K_S^0 \pi^+ \pi^0$ and $B^+ \rightarrow K^+ \pi^0 \pi^0$ Dalitz planes.
- The CP-averaged $\mathcal{B}^{0+} = \text{BR}(B^+ \rightarrow K^{*0} \pi^+)$ branching fraction and its corresponding CP asymmetry A_{CP}^{0+} . They can be measured both in the $B^+ \rightarrow K^+ \pi^+ \pi^-$ and $B^+ \rightarrow K_S^0 \pi^0 \pi^+$ Dalitz planes.
- The phase difference $\varphi^{00,+}$ between $B^0 \rightarrow K^{*+} \pi^-$ and $B^0 \rightarrow K^{*0} \pi^0$, and its corresponding CP conjugate $\bar{\varphi}^{00,-}$. They can be measured in the $B^0 \rightarrow K^+ \pi^- \pi^0$ Dalitz plane and in its CP-conjugate DP $\bar{B}^0 \rightarrow K^- \pi^+ \pi^0$, respectively.
- The phase difference $\varphi^{+0,0}$ between $B^+ \rightarrow K^{*+} \pi^0$ and $B^+ \rightarrow K^{*0} \pi^+$, and its corresponding CP conjugate $\bar{\varphi}^{-0,0}$. They can be measured in the $B^+ \rightarrow$

$K_S^0 \pi^+ \pi^0$ Dalitz plane and in its CP-conjugate DP $B^- \rightarrow K_S^0 \pi^- \pi^0$, respectively.

- The phase difference $\Delta\varphi^{+-}$ between $B^0 \rightarrow K^{*+} \pi^-$ and its CP conjugate $\bar{B}^0 \rightarrow K^{*-} \pi^+$. This phase difference can only be measured in a time-dependent analysis of the $K_S^0 \pi^+ \pi^-$ DP. As $K^{*+} \pi^-$ is only accessible for B^0 and $K^{*-} \pi^+$ to \bar{B}^0 only, the $B^0 \rightarrow K^{*+} \pi^-$ and $\bar{B}^0 \rightarrow K^{*-} \pi^+$ amplitudes do not interfere directly (they contribute to different DPs). But they do interfere with intermediate resonant amplitudes that are accessible to both B^0 and \bar{B}^0 , like $\rho^0(770)K_S^0$ or $f_0(980)K_S^0$, and thus the time-dependent oscillation is sensitive to the combined phases from mixing and decay amplitudes.

2.1 Real-valued physical observables

The set of physical observables described in the previous paragraph (branching fractions, CP asymmetries and phase differences) has the advantage of providing straightforward physical interpretations. From a technical point of view though, the phase differences suffer from the drawback of their definition with a 2π periodicity. This feature becomes an issue when the experimental uncertainties on the phases are large and the correlations between observables are significant, since there is no straightforward way to properly implement their covariance into a fit algorithm. Moreover, the uncertainties on the phases are related to the moduli of the corresponding amplitudes, leading to problems when the latter are not known precisely and can reach values compatible with zero. As a solution to this issue, a set of real-valued Cartesian physical observables is defined, in which the CP asymmetries and phase differences are expressed in terms of the real and imaginary parts of ratios of isobar amplitudes scaled by the ratios of the corresponding branching fractions and CP asymmetries. The new observables are functions of branching fractions, CP asymmetries and phase differences, and they are thus physical observables. The new set of observables, similar to the U and I observables defined in $B \rightarrow \rho \pi$ [5], are expressed as the real and imaginary parts of ratios of amplitudes as follows:

$$\text{Re}(A_i/A_j) = \sqrt{\frac{\mathcal{B}^i A_{\text{CP}}^i - 1}{\mathcal{B}^j A_{\text{CP}}^j - 1}} \cos(\varphi_{ij}), \tag{6}$$

$$\text{Im}(A_i/A_j) = \sqrt{\frac{\mathcal{B}^i A_{\text{CP}}^i - 1}{\mathcal{B}^j A_{\text{CP}}^j - 1}} \sin(\varphi_{ij}), \tag{7}$$

$$\text{Re}(\bar{A}_i/\bar{A}_j) = \sqrt{\frac{\mathcal{B}^i A_{\text{CP}}^i + 1}{\mathcal{B}^j A_{\text{CP}}^j + 1}} \cos(\bar{\varphi}_{ij}), \tag{8}$$

$$\text{Im}(\bar{A}_i/\bar{A}_j) = \sqrt{\frac{\mathcal{B}^i A_{\text{CP}}^i + 1}{\mathcal{B}^j A_{\text{CP}}^j + 1}} \sin(\bar{\varphi}_{ij}). \quad (9)$$

We see that some observables are not defined in the case $A_{\text{CP}}^j = \pm 1$, as could be expected from the following argument. Let us suppose that $A_{\text{CP}}^j = +1$ for the j th resonance, i.e., we have the amplitude $A_j = 0$: the quantities $\text{Re}(A_i/A_j)$ and $\text{Im}(A_i/A_j)$ are not defined, but neither is the phase difference between A_i and A_j . Therefore, in both parametrisations (real and imaginary part of ratios, or branching ratios, CP asymmetries and phase differences), the singular case $A_{\text{CP}}^j = \pm 1$ leads to some undefined observables. Let us add that this case does not occur in practice for our analysis.

For each $B \rightarrow K\pi\pi$ mode considered in this paper, the real and imaginary parts of amplitude ratios used as inputs are the following:

$$B^0 \rightarrow K_S^0 \pi^+ \pi^- : \quad (10)$$

$$\mathcal{B}(K^{*+} \pi^-);$$

$$\text{Re} \left[\frac{q \bar{A}(K^{*-} \pi^+)}{p A(K^{*+} \pi^-)} \right]; \quad \text{Im} \left[\frac{q \bar{A}(K^{*-} \pi^+)}{p A(K^{*+} \pi^-)} \right],$$

$$B^0 \rightarrow K^+ \pi^- \pi^0 : \quad (11)$$

$$\left\{ \begin{array}{l} \mathcal{B}(K^{*0} \pi^0); \quad \left| \frac{\bar{A}(K^{*-} \pi^+)}{A(K^{*+} \pi^-)} \right|; \\ \text{Re} \left[\frac{A(K^{*0} \pi^0)}{A(K^{*+} \pi^-)} \right]; \quad \text{Im} \left[\frac{A(K^{*0} \pi^0)}{A(K^{*+} \pi^-)} \right]; \\ \text{Re} \left[\frac{\bar{A}(K^{*0} \pi^0)}{A(K^{*-} \pi^+)} \right]; \quad \text{Im} \left[\frac{\bar{A}(K^{*0} \pi^0)}{A(K^{*-} \pi^+)} \right], \end{array} \right.$$

$$B^+ \rightarrow K^+ \pi^- \pi^+ : \quad (12)$$

$$\mathcal{B}(K^{*0} \pi^+); \quad \left| \frac{\bar{A}(K^{*0} \pi^-)}{A(K^{*0} \pi^+)} \right|,$$

$$B^+ \rightarrow K_S^0 \pi^+ \pi^0 : \quad (13)$$

$$\left\{ \begin{array}{l} \mathcal{B}(K^{*+} \pi^0); \quad \left| \frac{\bar{A}(K^{*-} \pi^0)}{A(K^{*+} \pi^0)} \right|; \\ \text{Re} \left[\frac{A(K^{*+} \pi^0)}{A(K^{*0} \pi^+)} \right]; \quad \text{Im} \left[\frac{A(K^{*+} \pi^0)}{A(K^{*0} \pi^+)} \right]; \\ \text{Re} \left[\frac{\bar{A}(K^{*-} \pi^0)}{A(K^{*0} \pi^-)} \right]; \quad \text{Im} \left[\frac{\bar{A}(K^{*-} \pi^0)}{A(K^{*0} \pi^-)} \right]. \end{array} \right.$$

This choice of inputs is motivated by the fact that amplitude analyses are sensitive to ratios of isobar amplitudes. The sensitivity to phase differences leads to a sensitivity to the real and imaginary part of these ratios. It has to be said that the set of inputs listed previously is just one of the possible sets of independent observables that can be extracted from this set of amplitude analyses. In order to combine BABAR and Belle results, it is straightforward to express the experimental results in the above format, and then combine them as

is done for independent measurements. Furthermore, experimental information from other analyses which are not amplitude and/or time-dependent, i.e., which are only sensitive to \mathcal{B} and A_{CP} , can also be added in a straightforward fashion.

In order to properly use the experimental information in the above format it will be necessary to use the full covariance matrix, both statistical and systematic, of the isobar amplitudes. This will allow us to properly propagate the uncertainties as well as the correlations of the experimental inputs to the ones exploited in the phenomenological fit.

3 Isospin analysis of $B \rightarrow K^* \pi$ decays

The isospin formalism used in this work is described in detail in Ref. [51]. Only the main ingredients are summarised below.

Without any loss of generality, exploiting the unitarity of the CKM matrix, the $B^0 \rightarrow K^{*+} \pi^-$ decay amplitude A^{+-} can be parametrised as

$$A^{+-} = V_{ub}^* V_{us} T^{+-} + V_{tb}^* V_{ts} P^{+-}, \quad (14)$$

with similar expressions for the CP-conjugate amplitude \bar{A}^{-+} (the CKM factors appearing as complex conjugates), and for the remaining three amplitudes $A^{ij} = A(B^{i+j} \rightarrow K^{*i} \pi^j)$, corresponding to the $(i, j) = (0, +), (+, 0), (00)$ modes. The tree and penguin contributions are now defined through their CKM factors rather than their diagrammatic structure: they can include contributions from additional c -quark penguin diagrams due to the re-expression of $V_{cb}^* V_{cs}$ in Eq. (14). In the following, T^{ij} and P^{ij} will be called hadronic amplitudes.

Note that the relative CKM matrix elements in Eq. (14) significantly enhance the penguin contributions with respect to the tree ones, providing an improved sensitivity to the former. The isospin invariance imposes a quadrilateral relation among these four decay amplitudes, derived in Ref. [52] for $B \rightarrow K\pi$, but equivalently applicable in the $K^* \pi$ case:

$$A^{0+} + \sqrt{2} A^{+0} = A^{+-} + \sqrt{2} A^{00}, \quad (15)$$

and a similar expression for the CP-conjugate amplitudes. These can be used to rewrite the decay amplitudes in the ‘‘canonical’’ parametrisation,

$$A^{+-} = V_{us} V_{ub}^* T^{+-} + V_{ts} V_{tb}^* P^{+-},$$

$$A^{0+} = V_{us} V_{ub}^* N^{0+} + V_{ts} V_{tb}^* (-P^{+-} + P_{\text{EW}}^{\text{C}}),$$

$$\sqrt{2} A^{+0} = V_{us} V_{ub}^* T^{+0} + V_{ts} V_{tb}^* P^{+0},$$

$$\sqrt{2} A^{00} = V_{us} V_{ub}^* T_{\text{C}}^{00} + V_{ts} V_{tb}^* (-P^{+-} + P_{\text{EW}}), \quad (16)$$

with

$$T^{+0} = T^{+-} + T_C^{00} - N^{0+}, \tag{17}$$

$$P^{+0} = P^{+-} + P_{EW} - P_{EW}^C. \tag{18}$$

This parametrisation is frequently used in the literature with various slightly different conventions, and is expected to hold up to a very high accuracy (see Refs. [53,58] for isospin-breaking contributions to $B \rightarrow \pi\pi$ decays). The notation is chosen to illustrate the main diagram topologies contributing to the decay amplitude under consideration. N^{0+} makes reference to the fact that the contribution to $B^+ \rightarrow K^{*0}\pi^+$ with a $V_{us}V_{ub}^*$ term corresponds to an annihilation/exchange topology; T_C^{00} denotes the colour-suppressed $B^0 \rightarrow K^{*0}\pi^0$ tree amplitude; the EW subscript in the P_{EW} and P_{EW}^C terms refers to the $\Delta I = 1$ electroweak penguin contributions to the decay amplitudes. We can also introduce the $\Delta I = 3/2$ combination $T_{3/2} = T^{+-} + T_C^{00}$.

One naively expects that colour-suppressed contributions will indeed be suppressed compared to their colour-allowed partner, and that electroweak penguins and annihilation contributions will be much smaller than tree and QCD penguins. These expectations can be expressed quantitatively using theoretical approaches like QCD factorisation [14–17]. Some of these assumptions have been challenged by the experimental data gathered, in particular the mechanism of colour suppression in $B \rightarrow \pi\pi$ and the smallness of the annihilation part for $B \rightarrow K\pi$ [5,22,37,55–57].

The complete set of $B \rightarrow K^*\pi$ decay amplitudes, constrained by the isospin relations described in Eq. (15) are fully described by 13 parameters, which can be classified as 11 hadronic and 2 CKM parameters following Eq. (16). A unique feature of the $B \rightarrow K^*\pi$ system is that this number of unknowns matches the total number of physical observables discussed in Sect. 2. One could thus expect that all parameters (hadronic and CKM) could be fixed from the data. However, it turns out that the weak and strong phases can be redefined in such a way as to absorb in the CKM parameters any constraints on the hadronic ones. This property, known as reparametrisation invariance, is derived in detail in Refs. [51,54] and we recall its essential aspects here. The decay amplitude of a B meson into a final state can be written as

$$A_f = m_1 e^{i\phi_1} e^{i\delta_1} + m_2 e^{i\phi_2} e^{i\delta_2}, \tag{19}$$

$$\bar{A}_{\bar{f}} = m_1 e^{-i\phi_1} e^{i\delta_1} + m_2 e^{-i\phi_2} e^{i\delta_2}, \tag{20}$$

where ϕ_i are CP-odd (weak) phases, δ_i are CP-even (strong) phases, and m are real magnitudes. Any additional term $M_3 e^{i\phi_3} e^{i\delta_3}$ can be expressed as a linear combination of $e^{i\phi_1}$ and $e^{i\phi_2}$ (with the appropriate properties under CP violation), leading to the fact that the decay amplitudes can be written in terms of any other pair of weak phases $\{\varphi_1, \varphi_2\}$ as long as

$\varphi_1 \neq \varphi_2 \pmod{\pi}$:

$$A_f = M_1 e^{i\varphi_1} e^{i\Delta_1} + M_2 e^{i\varphi_2} e^{i\Delta_2}, \tag{21}$$

$$\bar{A}_{\bar{f}} = M_1 e^{-i\varphi_1} e^{i\Delta_1} + M_2 e^{-i\varphi_2} e^{i\Delta_2}, \tag{22}$$

with

$$M_1 e^{i\Delta_1} = [m_1 e^{i\delta_1} \sin(\phi_1 - \varphi_2) + m_2 e^{i\delta_2} \sin(\phi_2 - \varphi_2) / \sin(\varphi_2 - \varphi_1)], \tag{23}$$

$$M_2 e^{i\Delta_2} = [m_1 e^{i\delta_1} \sin(\phi_1 - \varphi_1) + m_2 e^{i\delta_2} \sin(\phi_2 - \varphi_1)] / \sin(\varphi_2 - \varphi_1). \tag{24}$$

This change in the set of weak basis does not have any physical implications, hence the name of re-parameterisation invariance. We can now take two different sets of weak phases $\{\phi_1, \phi_2\}$ and $\{\varphi_1, \varphi_2\}$ with $\phi_1 = \varphi_1$ but $\phi_2 \neq \varphi_2$. If an algorithm existed to extract ϕ_2 as a function of physical observables related to these decay amplitudes, the similarity of Eqs. (19), (20) and (21), (22) indicate that φ_2 would be extracted exactly using the same function with the same measurements as input, leading to $\varphi_2 = \phi_2$, in contradiction with the original statement that we are free to express the physical observables using an arbitrary choice for the weak basis.

We have thus to abandon the idea of an algorithm allowing one to extract both CKM and hadronic parameters from a set of physical observables. The weak phases in the parameterisation of the decay amplitudes cannot be extracted without additional hadronic hypothesis. This discussion holds if the two weak phases used to describe the decay amplitudes are different (modulo ϕ). The argument does not apply when only one weak phase can be used to describe the decay amplitude: setting one of the amplitudes to zero, say $m_2 = 0$, breaks reparametrisation invariance, as can be seen easily in Eqs. (23) and (24). In such cases, weak phases can be extracted from experiment, e.g., the extraction of α from $B \rightarrow \pi\pi$, the extraction of β from $J/\psi K_S$ or γ from $B \rightarrow DK$. In each case, an amplitude is assumed to vanish, either approximately (extraction of α and β) or exactly (extraction of γ) [1,2,5].

In view of this limitation, two main strategies can be considered for the system considered here: either implementing additional constraints on some hadronic parameters in order to extract the CKM phases using the $B \rightarrow K^*\pi$ observables, or fix the CKM parameters to their known values from a global fit and use the $B \rightarrow K^*\pi$ observables to extract information on the hadronic contributions to the decay amplitudes. Both approaches are described below.

4 Constraints on CKM phases

We illustrate the first strategy using two specific examples. The first example is similar in spirit to the Gronau–London

method for extracting the CKM angle α [59], which relies on neglecting the contributions of electroweak penguins to the $B \rightarrow \pi\pi$ decay amplitudes. The second example assumes that upper bounds on annihilation/exchange contributions can be estimated from external information.

4.1 The CPS/GPSZ method: setting a bound on electroweak penguins

In $B \rightarrow \pi\pi$ decays, the electroweak penguin contribution can be related to the tree amplitude in a model-independent way using Fierz transformations of the relevant current–current operators in the effective Hamiltonian for $B \rightarrow \pi\pi$ decays [6, 60–62]. One can predict the ratio $R = P_{EW}/T_{3/2} \simeq -3/2(C_9 + C_{10})/(C_1 + C_2) = (1.35 \pm 0.12)\%$ only in terms of short-distance Wilson Coefficients, since long-distance hadronic matrix elements drop from the ratio (neglecting the operators O_7 and O_8 due to their small Wilson coefficients compared to O_9 and O_{10}). This leads to the prediction that there is no strong phase difference between P_{EW} and $T_{3/2}$ so that electroweak penguins do not generate a charge asymmetry in $B^+ \rightarrow \pi^+\pi^0$ if this picture holds: this prediction is in agreement with the present experimental average of the corresponding asymmetry. Moreover, this assumption is crucial to ensure the usefulness of the Gronau–London method to extract the CKM angle α from an isospin analysis of $B \rightarrow \pi\pi$ decay amplitudes [5, 6]: setting the electroweak penguin to zero in the Gronau–London breaks the reparametrisation invariance described in Sect. 3 and opens the possibility of extracting weak phases.

One may want to follow a similar approach and use some knowledge or assumptions on the electroweak penguin in the case of $B \rightarrow K\pi$ or $B \rightarrow K^*\pi$ in order to constrain the CKM factors. This approach is sometimes referred to as the CPS/GPSZ method [64, 65]. Indeed, as shown in Eq. (16), the penguins in A^{00} and A^{+-} differ only by the P_{EW} term. By neglecting its contribution to A^{00} , these two decay amplitudes can be combined so that their (now identical) penguin terms can be eliminated,

$$A^0 = A^{+-} + \sqrt{2}A^{00} = V_{us}V_{ub}^*(T^{+-} + T_C^{00}), \quad (25)$$

and then, together with its CP-conjugate amplitude \bar{A}^0 , a convention-independent amplitude ratio R^0 can be defined as

$$R^0 = \frac{q}{p} \frac{\bar{A}^0}{A^0} = e^{-2i\beta} e^{-2i\gamma} = e^{2i\alpha}. \quad (26)$$

The A^0 amplitude can be extracted using the decay chains $B^0 \rightarrow K^{*+}(\rightarrow K^+\pi^0)\pi^-$ and $B^0 \rightarrow K^{*0}(\rightarrow K^+\pi^-)\pi^0$ contributing to the same $B^0 \rightarrow K^+\pi^-\pi^0$ Dalitz plot, so that both the partial decay rates and their interference phase can be measured in an amplitude analysis. Similarly, \bar{A}^0 can be extracted from the CP-conjugate $\bar{B}^0 \rightarrow K^-\pi^+\pi^0$ DP

using the same procedure. Then the phase difference between A^{+-} and \bar{A}^{-+} can be extracted from the $B^0 \rightarrow K_S^0\pi^+\pi^-$ DP, considering the $B^0 \rightarrow K^{*+}(\rightarrow K^0\pi^+)\pi^-$ decay chain, and its CP-conjugate $\bar{B}^0 \rightarrow K^{*-}(\rightarrow \bar{K}^0\pi^-)\pi^+$, which do interfere through mixing. Let us stress that this method is a measurement of α rather than a measurement of γ , in contrast with the claims in Refs. [64, 65].

However, the method used to bound P_{EW} for the $\pi\pi$ system cannot be used directly in the $K^*\pi$ case. In the $\pi\pi$ case, $SU(2)$ symmetry guarantees that the matrix element with the combination of operators $O_1 - O_2$ vanishes, so that it does not enter tree amplitudes. A similar argument would hold for $SU(3)$ symmetry in the case of the $K\pi$ system, but it does not for the vector–pseudo-scalar $K^*\pi$ system. It is thus not possible to cancel hadronic matrix elements when considering $P_{EW}/T_{3/2}$, which becomes a complex quantity suffering from (potentially large) hadronic uncertainties [63, 64]. The size of the electroweak penguin (relative to the tree contributions), is parametrised as

$$\frac{P_{EW}}{T_{3/2}} = R \frac{1 - r_{VP}}{1 + r_{VP}}, \quad (27)$$

where $R \simeq (1.35 \pm 0.12)\%$ is the value obtained in the $SU(3)$ limit for $B \rightarrow \pi K$ (and identical to the one obtained from $B \rightarrow \pi\pi$ using the arguments in Refs. [60–62]), and r_{VP} is a complex parameter measuring the deviation of $P/T_{3/2}$ from this value corresponding to

$$r_{VP} = \frac{\langle K^*\pi(I=3/2)|Q_1 - Q_2|B \rangle}{\langle K^*\pi(I=3/2)|Q_1 + Q_2|B \rangle}. \quad (28)$$

Estimates on factorisation and/or $SU(3)$ flavour relations suggest $|r_{VP}| \leq 0.05$ [64, 65]. However, it is clear that both approximations can easily be broken, suggesting a more conservative upper bound $|r_{VP}| \leq 0.30$.

The presence of these hadronic uncertainties have important consequences for the method. Indeed, it turns out that including a non-vanishing P_{EW} completely disturbs the extraction of α . The electroweak penguin can provide a $\mathcal{O}(1)$ contribution to CP-violating effects in charmless $b \rightarrow s$ processes, as its CKM coupling amplifies its contribution to the decay amplitude: P_{EW} is multiplied by a large CKM factor $V_{ts}V_{tb}^* = \mathcal{O}(\lambda^2)$ compared to the tree-level amplitudes multiplied by a CKM factor $V_{us}V_{ub}^* = \mathcal{O}(\lambda^4)$. Therefore, unless P_{EW} is particularly suppressed due to some specific hadronic dynamics, its presence modifies the CKM constraint obtained following this method in a very significant way.

It would be difficult to illustrate this point using the current data, due to the experimental uncertainties described in the next sections. We choose thus to discuss this problem using a reference scenario described in Table 11, where the hadronic amplitudes have been assigned arbitrary (but realis-

tic) values and they are used to derive a complete set of experimental inputs with arbitrary (and much more precise than currently available) uncertainties. As shown in Appendix A (cf. Table 11), the current world averages for branching ratios and CP asymmetries in $B^0 \rightarrow K^{*+}\pi^-$ and $B^0 \rightarrow K^{*0}\pi^0$ agree broadly with these values, which also reproduce the expected hierarchies among hadronic amplitudes, if we set the CKM parameters to their current values from our global fit [6–8]. We choose a penguin parameter P^{+-} with a magnitude 28 times smaller than the tree parameter T^{+-} , and a phase fixed at -7° . The electroweak P_{EW} parameter has a value 66 times smaller in magnitude than the tree parameter T^{+-} , and its phase is arbitrarily fixed to $+15^\circ$ in order to get good agreement with the current central values. Our results do not depend significantly on this phase, and a similar outcome occurs if we choose sets with a vanishing phase for P_{EW} (though the agreement with the current data will be less good).

We use the values of the observables derived with this set of hadronic parameters, and we perform a CPS/GPSZ analysis to extract a constraint on the CKM parameters. Figure 1 shows the constraints derived in the $\bar{\rho}-\bar{\eta}$ plane. If we assume $P_{EW} = 0$ (upper panel), the extracted constraint is equivalent to a constraint on the CKM angle α , as expected from Eq. (26). However, the confidence regions in the $\bar{\rho}-\bar{\eta}$ plane are very strongly biased, and the true value of the parameters are far from belonging to the 95% confidence regions. On the other hand, if we fix P_{EW} to its true value (with a magnitude of 0.038), the bias is removed but the constraint deviates from a pure α -like shape (for instance, it does not include the origin point $\bar{\rho} = \bar{\eta} = 0$). We notice that the uncertainties on R and, more significantly, r_{VP} , have an important impact on the precision of the constraint on $(\bar{\rho}, \bar{\eta})$.

This simple illustration with our reference scenario shows that the CPS/GPSZ method is limited both in robustness and accuracy due to the assumption on a negligible P_{EW} : a small non-vanishing value breaks the relation between the phase of R^0 and the CKM angle α , and therefore, even a small uncertainty on the P_{EW} value would translate into large biases on the CKM constraints. It shows that this method would require a very accurate understanding of hadronic amplitudes in order to extract a meaningful constraint on the unitarity triangle, and the presence of non-vanishing electroweak penguins dilutes the potential of this method significantly.

4.2 Setting bounds on annihilation/exchange contributions

As discussed in the previous paragraphs, the penguin contributions for $B \rightarrow K^*\pi$ decays are strongly CKM-enhanced, impacting the CPS/GPSZ method based on neglecting a penguin amplitude P_{EW} . This method exhibits a strong sensitivity to small changes or uncertainties in values assigned to the electroweak penguin contribution. An alternative and safer

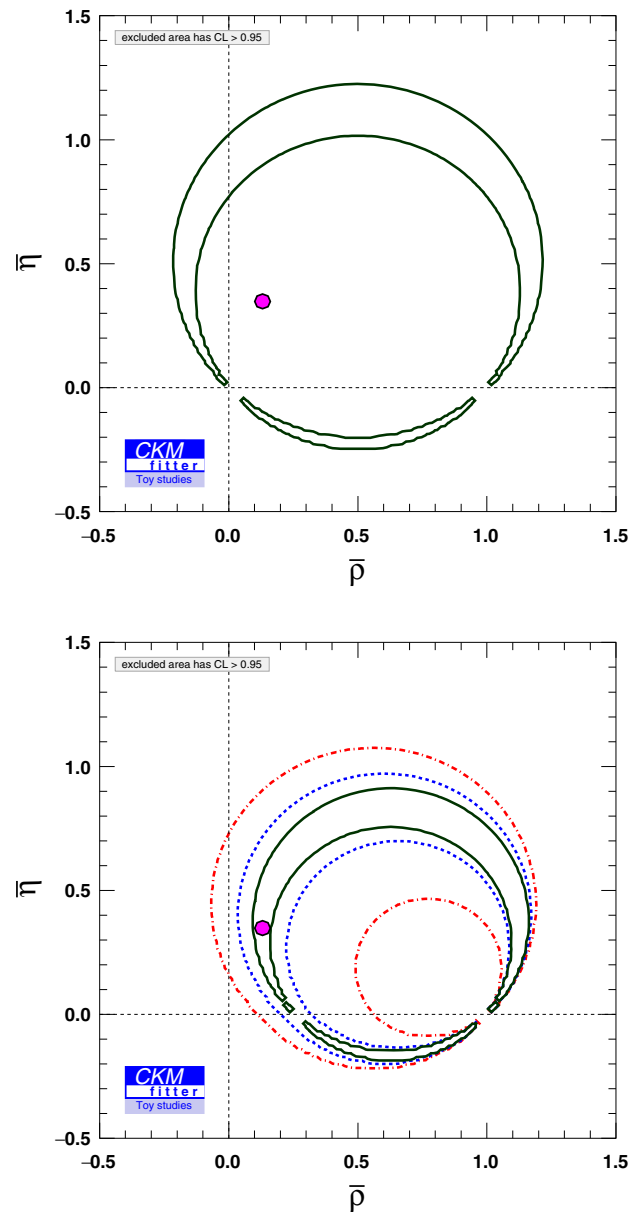


Fig. 1 Constraints in the $\bar{\rho}-\bar{\eta}$ plane from the amplitude ratio R^0 method, using the arbitrary but realistic numerical values for the input parameters, detailed in the text. In the *top panel*, the P_{EW} hadronic parameter is set to zero. In the *bottom panel*, the P_{EW} hadronic parameter is set to its true generation value with different theoretical errors on R and r_{VP} parameters [defined in Eq. (27)], either zero (*green solid-line contour*), 10 and 5% (*blue dashed-line contour*), and 10 and 30% (*red solid-dashed-line contour*). The parameters $\bar{\rho}$ and $\bar{\eta}$ are fixed to their current values from the global CKM fit [6–8], indicated by the *magenta point*

approach consists in constraining a tree amplitude, with a CKM-suppressed contribution. Among the various hadronic amplitudes introduced, it seems appropriate to choose the annihilation amplitude N^{0+} , which is expected to be smaller than T^{+-} , and which could even be smaller than the colour-suppressed T_C^{00} . Unfortunately, no direct, clean constraints

on N^{0+} can be extracted from data and from the theoretical point of view, N^{0+} is dominated by incalculable non-factorisable contributions in QCD factorisation [14–17]. On the other hand, indirect upper bounds on N^{0+} may be inferred from either the $B^+ \rightarrow K^{*0}\pi^+$ decay rate or from the U -spin related mode $B^+ \rightarrow K^{*0}K^+$.

This method, like the previous one, hinges on a specific assumption on hadronic amplitudes. Fixing N^{0+} breaks the reparametrisation invariance in Sect. 3, and thus provides a way of measuring weak phases. We can compare the two approaches by using the same reference scenario as in Sect. 4.1, i.e., the values gathered in Table 11. We have an annihilation parameter N^{0+} with a magnitude 18 times smaller than the tree parameter T^{+-} , and a phase fixed at 108° . All $B \rightarrow K^*\pi$ physical observables are used as inputs. This time, all hadronic parameters are free to vary in the fits, except for the annihilation/exchange parameter N^{0+} , which is subject to two different hypotheses: either its value is fixed to its generation value, or the ratio $|N^{0+}/T^{+-}|$ is constrained in a range (up to twice its generation value).

The resulting constraints on $\bar{\rho}-\bar{\eta}$ are shown on the upper plot of Fig. 2. We stress that in this fit, the value of N^{0+} is bound, but the other amplitudes (including P_{EW}) are left free to vary. Using a loose bound on $|N^{0+}/T^{+-}|$ yields a less tight constraint, but in contrast with the CPS/GPSZ method, the CKM generation value is here included. One may notice that the resulting constraint is similar to the one corresponding to the CKM angle β . This can be understood in the following way. Let us assume that we neglect the contribution from N^{0+} . We obtain the following amplitude to be considered:

$$A' = A^{0+} = V_{ts} V_{tb}^* (-P^{+-} + P_{EW}^C), \quad (29)$$

and then, together with its CP-conjugate amplitude \bar{A}' , a convention-independent amplitude ratio R' can be defined as

$$R' = \frac{q}{p} \frac{\bar{A}'}{A'} = e^{-2i\beta}, \quad (30)$$

in agreement with the convention used to fix the phase of the B -meson state. This justifies the β -like shape of the constraint obtained when fixing the value of the annihilation parameter. The presence of the oscillation phase q/p here, starting from a decay of a charged B , may seem surprising. However, one should keep in mind that the measurement of $B^+ \rightarrow K^{*0}\pi^+$ and its CP-conjugate amplitude are not sufficient to determine the relative phase between A' and \bar{A}' : this requires one to reconstruct the whole quadrilateral equation Eq. (15), where the phases are provided by interferences between mixing and decay amplitudes in B_0 and \bar{B}_0 decays. In other words, the phase observables obtained from the Dalitz plot are always of the form Eqs. (4), (5): their com-

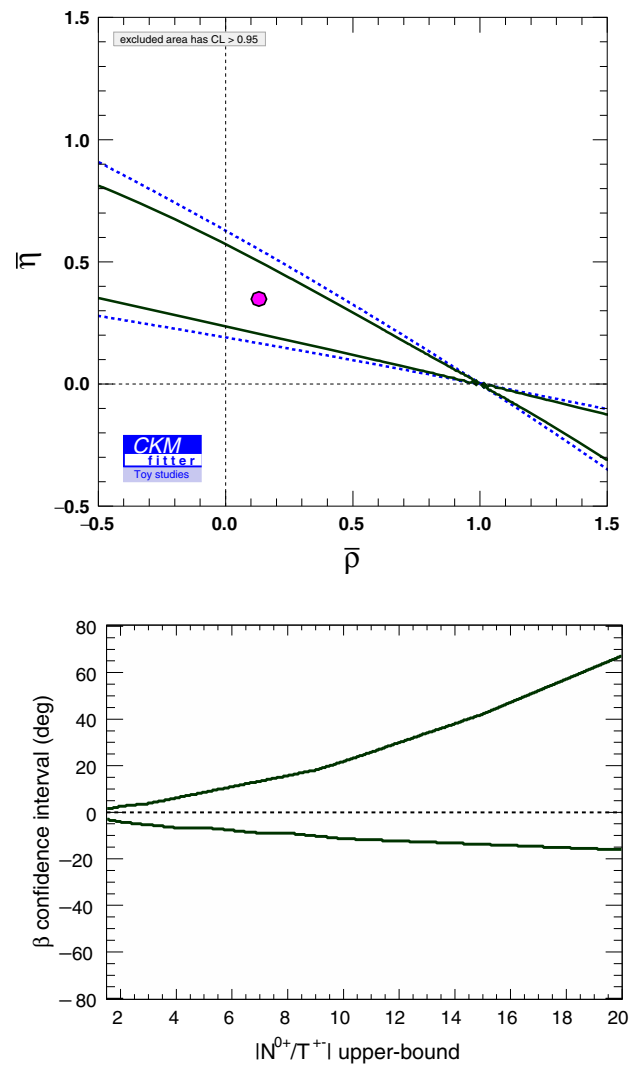


Fig. 2 Top constraints in the $\bar{\rho}-\bar{\eta}$ plane from the annihilation/exchange method, using the arbitrary but realistic numerical values for the input parameters detailed in the text. The green solid-line contour is the constraint obtained by fixing the N^{0+} hadronic parameter to its generation value; the blue dotted-line contour is the constraint obtained by setting an upper bound on the $|N^{0+}/T^{+-}|$ ratio at twice its generation value. The parameters $\bar{\rho}$ and $\bar{\eta}$ are fixed to their current values from the global CKM fit [6–8], indicated by the magenta point. Bottom size of the $\beta - \beta_{\text{gen}}$ 68% confidence interval vs. the upper bound on $|N^{0+}/T^{+-}|$ in units of its generation value.

ination can only lead to a ratio of CP-conjugate amplitudes multiplied by the oscillation parameter q/p .

The lower plot of Fig. 2 describes how the constraint on β loosens around its true value when the range allowed for $|N^{0+}/T^{+-}|$ is increased compared to its initial value (0.143). We see that the method is stable and keeps on including the true value for β even in the case of a mild constraint on $|N^{0+}/T^{+-}|$.

5 Constraints on hadronic parameters using current data

As already anticipated in Sect. 3, a second strategy to exploit the data consists in assuming that the CKM matrix is already well determined from the CKM global fit [6–8]. The measurements of $B \rightarrow K^* \pi$ observables (isobar parameters) can then be used to extract constraints on the hadronic parameters in Eq. (16).

5.1 Experimental inputs

For this study, the complete set of available results from the BABAR and Belle experiments is used. The level of detail for the publicly available results varies according to the decay mode in consideration. In most cases, at least one amplitude DP analysis of B^0 and B^+ decays is public [66], and at least one input from each physical observable is available. In addition, the conventions used in the various DP analyses are usually different. Ideally, one would like to have access to the complete covariance matrix, including statistical and systematic uncertainties, for all isobar parameters, as done for instance in Ref. [38]. Since such information is not always available, the published results are used in order to derive ad hoc approximate covariance matrices, implementing all the available information (central values, total uncertainties, correlations among parameters). The inputs for this study are the following:

- Two three-dimensional covariance matrices, cf. Eq. (10), from the BABAR time-dependent DP analysis of $B^0 \rightarrow K_S^0 \pi^+ \pi^-$ in Ref. [38], and two three-dimensional covariance matrices from the Belle time-dependent DP analysis of $B^0 \rightarrow K_S^0 \pi^+ \pi^-$ in Ref. [44]. Both the BABAR and Belle analyses found two quasi-degenerate solutions each, with very similar goodness-of-fit merits. The combination of these solutions is described in Appendix A.3, and is taken as input for this study.
- A five-dimensional covariance matrix, cf. Eq. (11), from the BABAR $B^0 \rightarrow K^+ \pi^- \pi^0$ DP analysis [40].
- A two-dimensional covariance matrix, cf. Eq. (12), from the BABAR $B^+ \rightarrow K^+ \pi^+ \pi^-$ DP analysis [39], and a two-dimensional covariance matrix from the Belle $B^+ \rightarrow K^+ \pi^+ \pi^-$ DP analysis [43].
- A simplified uncorrelated four-dimensional input, cf. Eq. (13), from the BABAR $B^+ \rightarrow K_S^0 \pi^+ \pi^0$ preliminary DP analysis [41].

Besides the inputs described previously, there are other experimental measurements on different three-body final states performed in the quasi-two-body approach, which provide measurements of branching ratios and CP asymmetries only. Such is the case of the BABAR result on the

$B^+ \rightarrow K^+ \pi^0 \pi^0$ final state [42], where the branching ratio and the CP asymmetry of the $B^+ \rightarrow K^*(892)^+ \pi^0$ contribution are measured. In this study, these two measurements are treated as uncorrelated, and they are combined with the inputs from the DP analyses mentioned previously.

These sets of experimental central values and covariance matrices are described in Appendix A, where the combinations of the results from BABAR and Belle are also described.

Finally, we notice that the time-dependent asymmetry in $B \rightarrow K_S \pi^0 \pi^0$ has been measured [49,50]. As these are global analyses integrated over the whole DP, we cannot take these measurements into account. In principle a time-dependent isobar analysis of the $K_S \pi^0 \pi^0$ DP could be performed and it could bring about some independent information on $B \rightarrow K^{*0} \pi^0$ intermediate amplitudes. Since this more challenging analysis has not been done yet, we will not consider this channel for the time being.

5.2 Selected results for CP asymmetries and hadronic amplitudes

Using the experimental inputs described in Sect. 5.1, a fit to the complete set of hadronic parameters is performed. We discuss the fit results focusing on three aspects: the most significant direct CP asymmetries, the significance of electroweak penguins, and the relative hierarchies of hadronic contributions to the tree amplitudes. As will be seen in the following, the fit results can be interpreted in terms of two sets of local minima, out of which one yields constraints on the hadronic parameters in better agreement with the expectations from CPS/GPSZ, the measured direct CP asymmetries and the expected relative hierarchies of hadronic contributions.

5.2.1 Direct CP violation in $B^0 \rightarrow K^{*+} \pi^-$

The $B^0 \rightarrow K^{*+} \pi^-$ amplitude can be accessed both in the $B^0 \rightarrow K_S^0 \pi^+ \pi^-$ and $B^0 \rightarrow K^+ \pi^- \pi^0$ Dalitz-plot analyses. The direct CP asymmetry $A_{CP}(B^0 \rightarrow K^{*+} \pi^-)$ has been measured by BABAR in both modes [38,40] and by Belle in the $B^0 \rightarrow K_S^0 \pi^+ \pi^-$ mode [44]. All three measurements yield a negative value: incidentally, this matches also the sign of the two-body $B^0 \rightarrow K^+ \pi^-$ CP asymmetry, for which direct CP violation is clearly established.

Using the amplitude DP analysis results from these three measurements as inputs, the combined constraint on $A_{CP}(B^0 \rightarrow K^{*+} \pi^-)$ is shown in Fig. 3. The combined value is 3.0σ away from zero, and the 68% confidence interval on this CP asymmetry is 0.21 ± 0.07 approximately. This result is to be compared with the 0.23 ± 0.06 value provided by HFLAV [66]. The difference is likely to come from the fact that HFLAV performs an average of the CP asymmetries extracted from individual experiments, while this analysis

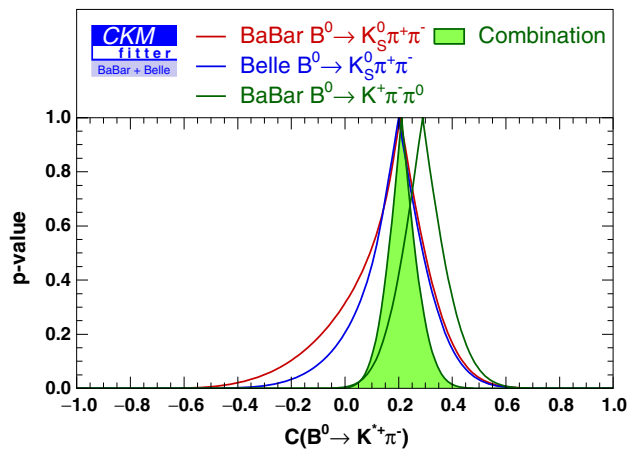


Fig. 3 Constraint on the direct CP asymmetry parameter $C(B^0 \rightarrow K^{*+}\pi^-) = -A_{CP}(B^0 \rightarrow K^{*+}\pi^-)$ from BABAR data on $B^0 \rightarrow K_S^0\pi^+\pi^-$ (red curve), Belle data on $B^0 \rightarrow K_S^0\pi^+\pi^-$ (blue curve), BABAR data on $B^0 \rightarrow K^+\pi^-\pi^0$ (green curve) and the combination of all these measurements (green shaded curve). The constraints are obtained using the observables described in the text

uses isobar values as inputs which are averaged over the various experiments before being translated into values for the CP parameters: since the relationships between these two sets of quantities are non-linear, the two steps (averaging over experiments and translating from one type of observables to another) yield the same central values only in the case of very small uncertainties. In the current situation, where sizeable uncertainties affect the determinations from individual experiments, it is not surprising that minor discrepancies arise between our approach and the HFLAV result.

As can be readily seen from Eq. (14), a non-vanishing asymmetry in this mode requires a strong phase difference between the tree T^{+-} and penguin P^{+-} hadronic parameters that is strictly different from zero. Figure 4 shows the two-dimensional constraint on the modulus and phase of the P^{+-}/T^{+-} ratio. Two solutions with very similar χ^2 are found, both incompatible with a vanishing phase difference. The first solution corresponds to a small (but non-vanishing) positive strong phase, with similar $|V_{ts}V_{tb}^*P^{+-}|$ and $|V_{us}V_{ub}^*T^{+-}|$ contributions to the total decay amplitude, and is called Solution I in the following. The other solution, denoted Solution II, corresponds to a larger, negative, strong phase, with a significantly larger penguin contribution. We notice that Solution I is closer to usual theoretical expectations concerning the relative size of penguin and tree contributions.

Let us stress that the presence of two solutions for P^{+-}/T^{+-} is not related to the presence of ambiguities in the individual BABAR and Belle measurements for $B^+ \rightarrow K^+\pi^+\pi^-$ and $B^0 \rightarrow K_S^0\pi^+\pi^-$, since we have performed their combinations in order to select a single solution for each process. Therefore, the presence of two solutions in Fig. 4 is

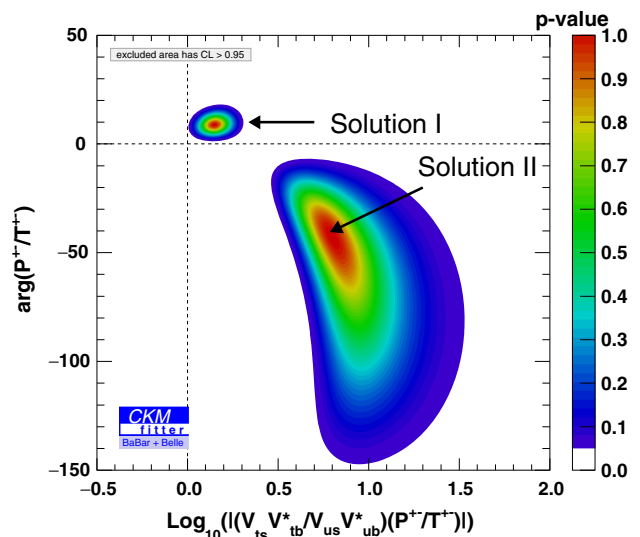


Fig. 4 Two-dimensional constraint on the modulus and phase of the P^{+-}/T^{+-} ratio. For convenience, the modulus is multiplied by the ratio of CKM factors appearing in the tree and penguin contributions to the $B^0 \rightarrow K^{*+}\pi^-$ decay amplitude

a global feature of our non-linear fit, arising from the overall structure of the current combined measurements (central values and uncertainties) that we use as inputs.

5.2.2 Direct CP violation in $B^+ \rightarrow K^{*+}\pi^0$

The $B^+ \rightarrow K^{*+}\pi^0$ amplitude can be accessed in a $B^+ \rightarrow K_S^0\pi^+\pi^0$ Dalitz-plot analysis, for which only a preliminary result from BABAR is available [41]. A large, negative CP asymmetry $A_{CP}(B^+ \rightarrow K^{*+}\pi^0) = -0.52 \pm 0.14 \pm 0.04_{-0.02}^{+0.04}$ is reported there with a 3.4σ significance. This CP asymmetry has also been measured by BABAR through a quasi-two-body analysis of the $B^+ \rightarrow K^+\pi^0\pi^0$ final state [42], obtaining $A_{CP}(B^+ \rightarrow K^{*+}\pi^0) = -0.06 \pm 0.24 \pm 0.04$. The combination of these two measurement yields $A_{CP}(B^+ \rightarrow K^{*+}\pi^0) = -0.39 \pm 0.12 \pm 0.03$, with a 3.2σ significance (Fig. 5).

In contrast with the $B^0 \rightarrow K^{*+}\pi^-$ case, in the canonical parametrisation Eq. (16), the decay amplitude for $B^+ \rightarrow K^{*+}\pi^0$ includes several hadronic contributions both to the total tree and penguin terms, namely

$$\begin{aligned} \sqrt{2}A^{+0} &= V_{us}V_{ub}^*T^{+0} + V_{ts}V_{tb}^*P^{+0} \\ &= V_{us}V_{ub}^*(T^{+-} + T_C^{00} - N^{0+}) \\ &\quad + V_{ts}V_{tb}^*(P^{+-} + P_{EW} - P_{EW}^C), \end{aligned} \tag{31}$$

and therefore no straightforward constraint on a single pair of hadronic parameters can be extracted, as several degenerate combinations can reproduce the observed value of the CP asymmetry $A_{CP}(B^+ \rightarrow K^{*+}\pi^0)$. This is illustrated in Fig. 6, where six different local minima are found in the

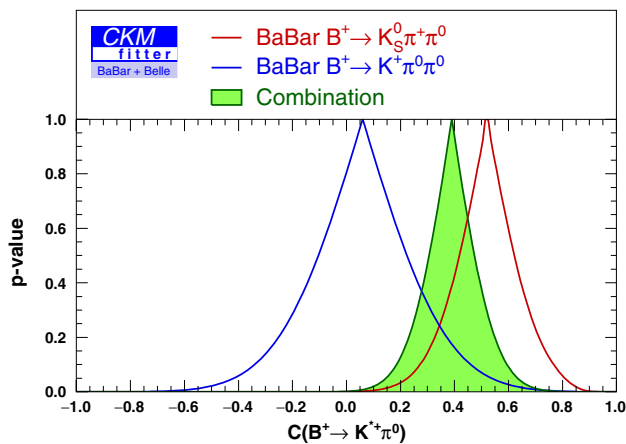


Fig. 5 Constraint on the direct CP asymmetry parameter $C(B^+ \rightarrow K^{*+}\pi^0) = -A_{CP}(B^+ \rightarrow K^{*+}\pi^0)$ from BABAR data on $B^+ \rightarrow K_S^0\pi^+\pi^0$ (red curve), BABAR data on $B^+ \rightarrow K^+\pi^0\pi^0$ (blue curve) and the combination (green shaded curve). The constraints are obtained using the observables described in the text

fit, all with similar χ^2 values. The three minima with positive strong phases correspond to Solution I, while the three minima with negative strong phases correspond to Solution II. The relative size of the total tree and penguin contributions is bound within a relatively narrow range: we get $|P^{+0}/T^{+0}| \in (0.018, 0.126)$ at 68% C.L.

5.2.3 Hierarchy among penguins: electroweak penguins

In Sect. 4.1, we described the CPS/GPSZ method designed to extract weak phases from $B \rightarrow \pi K$ assuming some control on the size of the electroweak penguin. According to this method, the electroweak penguin is expected to yield a small contribution to the decay amplitudes, with no significant phase difference. We are actually in a position to test this expectation by fitting the hadronic parameters using the BABAR and Belle data as inputs. Figure 7 shows the two-dimensional constraint on r_{VP} , in other words, the ratio $P_{EW}/T_{3/2}$ ratio, showing two local minima. The CPS/GPSZ prediction is also indicated in this figure. In Fig. 8, we provide the regions allowed for $|r_{VP}|$ and the modulus of the ratio $|P^{+-}/T^{+-}|$, exhibiting two favoured values, the smaller one being associated with Solution I and the larger one with Solution II. The latter one corresponds to a significantly large electroweak penguin amplitude and it is clearly incompatible with the CPS/GPSZ prediction by more than one order of magnitude. A better agreement, yet still marginal, is found for the smaller minimum that corresponds to Solution I: the central value for the ratio is about a factor of three larger than CPS/GPSZ, and a small, positive phase is preferred. For this minimum, an inflation of the uncertainty on $|r_{VP}|$ up to 30% would be needed to ensure proper agreement. In any case, it

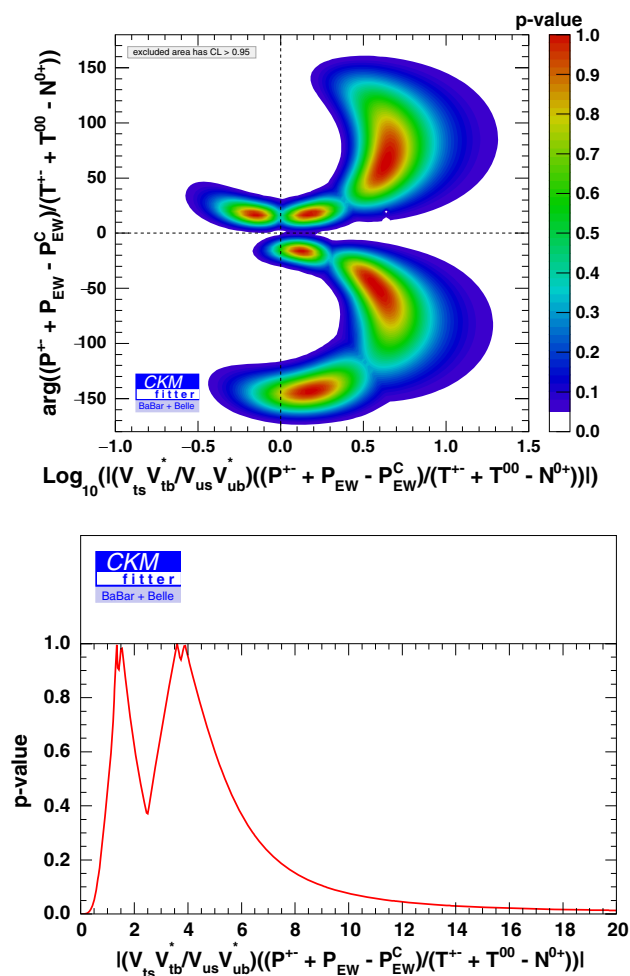


Fig. 6 Top two-dimensional constraint on the modulus and phase of the $(P^{+-} + P_{EW} - P_{EW}^C)/(T^{+-} + T_C^{00} - N^{0+})$ ratio. For convenience, the modulus is multiplied by the ratio of CKM factors appearing in the tree and penguin contributions to the $B^+ \rightarrow K^{*+}\pi^0$ decay amplitude. Bottom one-dimensional constraint on the modulus of the $(P^{+-} + P_{EW} - P_{EW}^C)/(T^{+-} + T_C^{00} - N^{0+})$ ratio

is clear that the data prefers a larger value of $|r_{VP}|$ than the estimates originally proposed.

Moreover, the contribution from the electroweak penguin is found to be about twice larger than the main penguin contribution P^{+-} . This is illustrated in Fig. 9, where only one narrow solution is found in the P_{EW}/P^{+-} plane, as both solutions I and II provide essentially the same constraint. The relative phase between these two parameters is bound to the interval $(-25, +10)^\circ$ at 95% C.L. Additional tests allow us to demonstrate that this strong constraint on the relative P_{EW}/P^{+-} penguin contributions is predominantly driven by the $\varphi^{00,+}$ phase differences measured in the BABAR Dalitz-plot analysis of $B^0 \rightarrow K^+\pi^+\pi^0$ decays. The strong constraint on the P_{EW}/P^{+-} ratio is turned into a mild upper bound when removing the $\varphi^{00,+}$ phase differences from the experimental inputs. The addition of these two observables

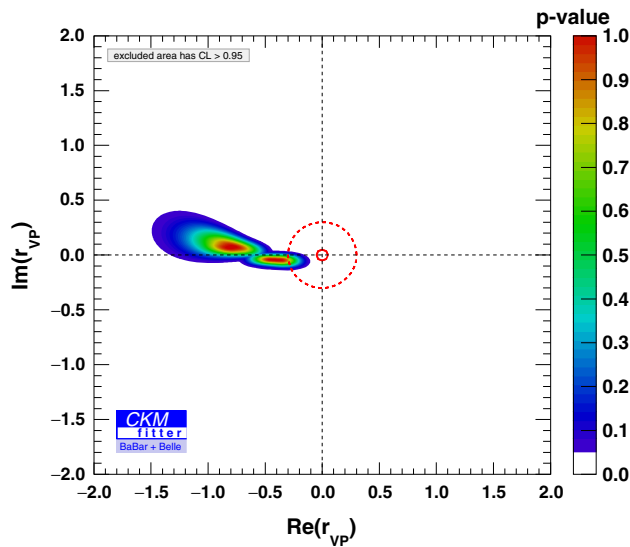


Fig. 7 Two-dimensional constraint on real and imaginary parts on the r_{VP} parameter defined in Eq. (27). The area encircled with the solid (dashed) red line corresponds to the CPS/GPSZ prediction, with a 5% (30%) uncertainty on the r_{VP} parameter

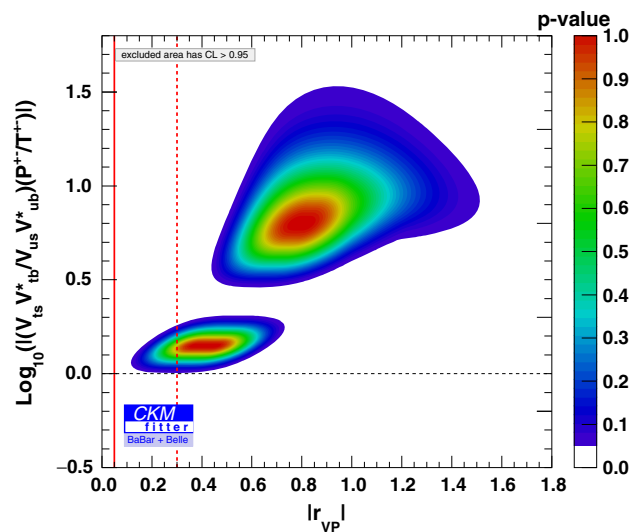


Fig. 8 Two-dimensional constraint on $|r_{VP}|$ defined in Eq. (27) and $\text{Log}_{10}(|(P^{+-}/T^{+-})|)$. The vertical solid (dashed) red line corresponds to the CPS/GPSZ prediction, with a 5% (30%) uncertainty

as fit inputs increases the minimal χ^2 by 7.7 units, which corresponds to a 2.6σ discrepancy. Since the latter is driven by a measurement from a single experiment, additional experimental results are needed to confirm such a large value for the electroweak penguin parameter.

In view of colour suppression, the electroweak penguin P_{EW}^C is expected to yield a smaller contribution than P_{EW} to the decay amplitudes. This hypothesis is tested in Fig. 10, which shows that current data favours a similar size for the two contributions, and a small relative phase (up to 40°) between the colour-allowed and the colour-suppressed elec-

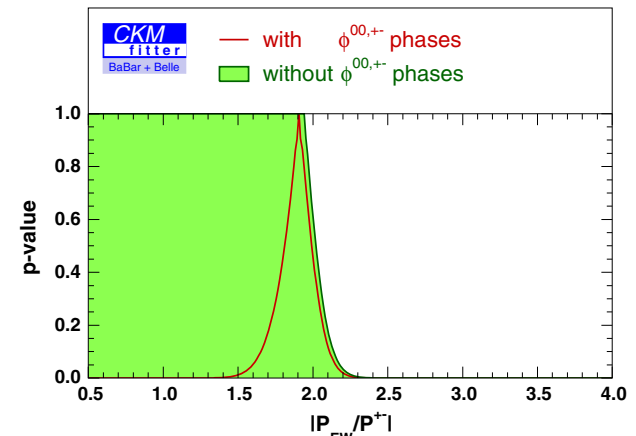
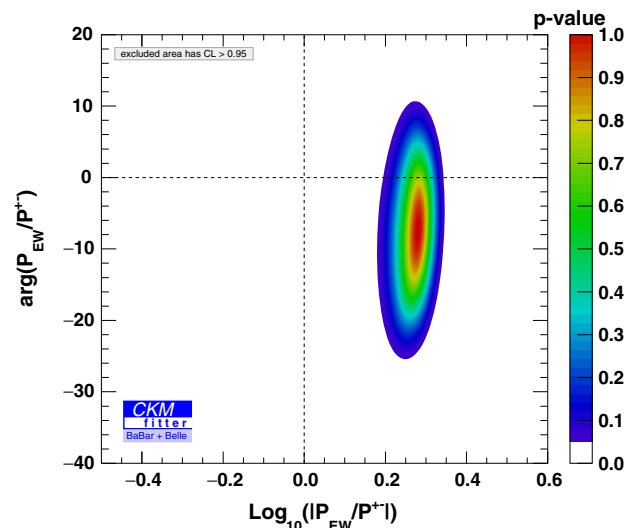


Fig. 9 Top two-dimensional constraint on the modulus and phase of the complex P_{EW}/P^{+-} ratio. Bottom constraint on the $|P_{EW}/P^{+-}|$ ratio, using the complete set of experimental inputs (red curve), and removing the BABAR measurement of the $\phi^{00,+}$ phases from the $B^0 \rightarrow K^+\pi^+\pi^0$ Dalitz-plot analysis (green shaded curve)

troweak penguins. Solutions I and II show the same structure with four different local minima.

5.2.4 Hierarchy among tree amplitudes: colour suppression and annihilation

As already discussed, the hadronic parameter T_C^{00} is expected to be suppressed with respect to the main tree parameter T^{+-} . Also, the annihilation topology is expected to provide negligible contributions to the decay amplitudes. These expectations can be compared with the extraction of these hadronic parameters from data in Fig. 11.

For colour suppression, the current data provides no constraint on the relative phase between the T_C^{00} and T^{+-} tree parameters, and only a mild upper bound on the modulus can be inferred; the tighter constraint is provided by Solu-

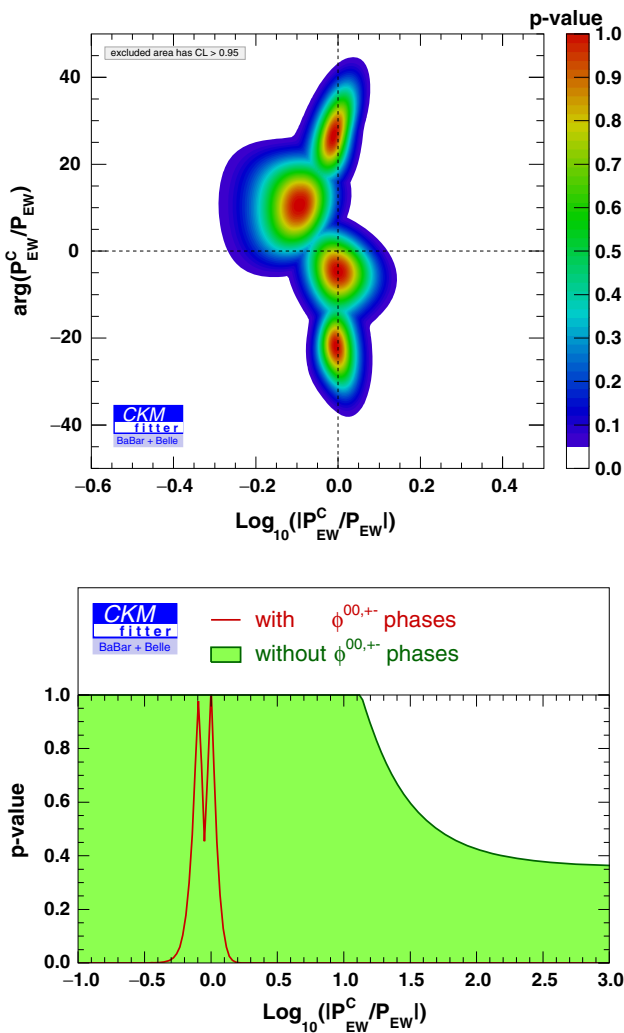


Fig. 10 Top two-dimensional constraint on the modulus and phase of the P_{EW}^C/P_{EW} ratio. Bottom one-dimensional constraint on $\text{Log}_{10}(|P_{EW}^C/P_{EW}|)$, using the complete set of experimental inputs (red curve), and removing the BABAR measurement of the $\phi^{00,+}$ phases from the $B^0 \rightarrow K^+\pi^+\pi^0$ Dalitz-plot analysis (green shaded curve)

tion I that excludes values of $|T_C^{00}/T^{+-}|$ larger than 1.6 at 95% C.L. The constraint from Solution II is more than one order of magnitude looser.

Similarly, for annihilation, Solution I provides slightly tighter constraints on its contribution to the total tree amplitude with the bound $|N^{0+}/T^{+-}| < 2.5$ at 95% C.L., while the bound from Solution II is much looser.

5.3 Comparison with theoretical expectations

We have extracted the values of the hadronic amplitudes from the data currently available. It may prove interesting to compare these results with theoretical expectations. For this exercise, we use QCD factorisation [14–17] as a benchmark point, keeping in mind that other approaches (discussed in the intro-

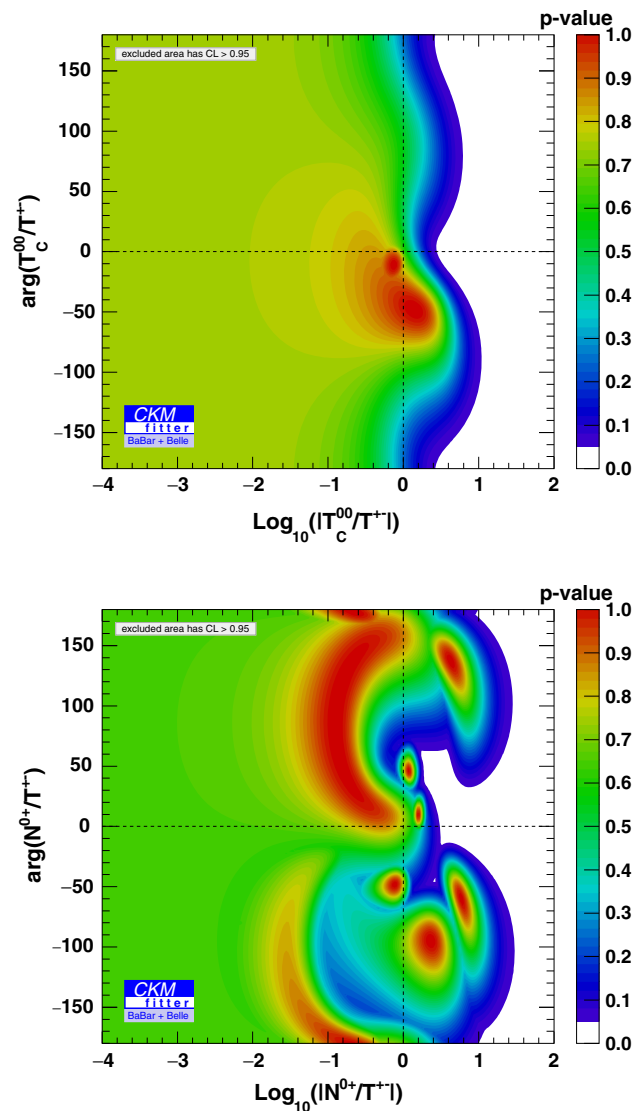


Fig. 11 Two-dimensional constraint on the modulus and phase of the T_C^{00}/T^{+-} (top) and N^{0+}/T^{+-} (bottom) ratios

duction) are available. In order to keep the comparison simple and meaningful, we consider the real and imaginary part of several ratios of hadronic amplitudes.

We obtain our theoretical values in the following way. We follow Ref. [16] for the expressions within QCD factorisation, and we use the same model for the power-suppressed and infrared-divergent contributions coming from hard scattering and weak annihilation: these contributions are formally $1/m_b$ -suppressed but numerically non-negligible, and play a crucial role in some of the amplitudes. On the other hand, we update the hadronic parameters in order to take into account more recent determinations of these quantities; see Appendix B. We use the Rfit scheme to handle theoretical uncertainties [6–8,67] (in particular for the hadronic parameters and the $1/m_b$ power-suppressed contributions),

and we compute only ratios of hadronic amplitudes using QCD factorisation. We stress that we provide the estimates within QCD factorisation simply to compare the results of our experimental fit for the hadronic amplitudes with typical theoretical expectations concerning the same quantities. In particular we neglect next-next-to-leading order corrections that have been partially computed in Refs. [57, 79–82], and we do not attempt to perform a fully combined fit of the theoretical predictions with the experimental data, as the large uncertainties would make the interpretation difficult.

Our results for the ratios of hadronic amplitudes are shown in Fig. 12 and in Table 1. We notice that for most of the ratios good agreement is found. The global fit to the experimental data has often much larger uncertainties than theoretical predictions: with better data in the future, we may be able to perform very non-trivial tests of the non-leptonic dynamics and the isobar approximation. The situation for P_{EW}^C/P_{EW} is slightly different, since the two determinations (experiment and theory) exhibit similar uncertainties and disagree with each other, providing an interesting test for QCD factorisation, which, however, goes beyond the scope of this study.

There are two cases where the theoretical output from QCD factorisation is significantly less precise than the constraints from the combined fit. For P_{EW}^C/P^{+-} , both numerator and denominator can be (independently) very small in QCD factorisation, and numerical instabilities in this ratio prevent us from having a precise prediction. For P^{+-}/P_{EW} , the impressively accurate experimental determination, as discussed in Sect. 5.2.3, is predominantly driven by the $\varphi^{00,+}$ phase differences measured in the BABAR Dalitz-plot analysis of $B^0 \rightarrow K^+\pi^+\pi^0$ decays. Removing this input yields a much milder constraint on P^{+-}/P_{EW} . On the other hand in QCD factorisation, the formally leading contributions to the P^{+-} penguin amplitude are somewhat numerically suppressed, and compete with the model estimate of power corrections: due to the Rfit treatment used, the two contributions can either compensate each other almost exactly or add up coherently, leading to a $\sim \pm 100$ relative uncertainty, which is only in marginal agreement with the fit output. Thus we conclude that the P^{+-}/P_{EW} ratio is both particularly sensitive to the power corrections to QCD factorisation and experimentally well constrained, so that it can be used to provide insight on non-factorisable contributions, provided one assumes negligible effects from New Physics.

6 Prospects for LHCb and Belle II

In this section, we study the impact of improved measurements of $K\pi\pi$ modes from the LHCb and Belle II experiments. During the first run of the LHC, the LHCb experiment has collected large datasets of B-hadron decays, including charmless B^0 , B^+ , B_s meson decays into tree-body modes.

LHCb is currently collecting additional data in Run-2. In particular, due to the excellent performances of the LHCb detector for identifying charged long-lived mesons, the experiment has the potential for producing the most accurate charmless three-body results in the $B^+ \rightarrow K^+\pi^-\pi^+$ mode, owing to high-purity event samples much larger than the ones collected by BABAR and Belle. Using 3.0 fb^{-1} of data recorded during the LHC Run 1, first results on this mode are already available [68], and a complete amplitude analysis is expected to be produced in the short-term future. For the $B^0 \rightarrow K_S^0\pi^+\pi^-$ mode, the event-collection efficiency is challenged by the combined requirements on reconstructing the $K_S^0 \rightarrow \pi^+\pi^-$ decay and tagging the B meson flavour, but nonetheless the $B^0 \rightarrow K_S^0\pi^+\pi^-$ data samples collected by LHCb are already larger than the ones from BABAR and Belle. As it is more difficult to anticipate the reach of LHCb Dalitz-plot analyses for modes including π^0 mesons in the final state, the $B^0 \rightarrow K^+\pi^+\pi^0$, $B^+ \rightarrow K_S^0\pi^+\pi^0$, $B^+ \rightarrow K^+\pi^0\pi^0$ and $B^0 \rightarrow K_S^0\pi^0\pi^0$ channels are not considered here. In addition, LHCb has also the potential for studying B_s decay modes, and LHCb can reach $B \rightarrow K K \pi$ modes with branching ratios out of reach for B -factories.

The Belle II experiment [69], currently in the stages of construction and commissioning, will operate in an experimental environment very similar to the one of the BABAR and Belle experiments. Therefore Belle II has the potential for studying all modes accessed by the B -factories, with expected sensitivities that should scale in proportion to its expected total luminosity (i.e., 50 ab^{-1}). In addition, Belle II has the potential for accessing the $B^+ \rightarrow K^+\pi^0\pi^0$ and $B^0 \rightarrow K_S^0\pi^0\pi^0$ modes (for which the B -factories could not produce Dalitz-plot results) but these modes will provide low-accuracy information, redundant with some of the modes considered in this paper: therefore they are not included here.

Since both LHCb and Belle II have the potential for studying large, high-quality samples of $B^+ \rightarrow K^+\pi^-\pi^+$, it is realistic to expect that the experiments will be able to extract a consistent, data-driven signal model to be used in all Dalitz-plot analysis, yielding systematic uncertainties significantly decreased with respect to the results from B -factories.

Finally for LHCb, since this experiment cannot perform B -meson counting as in a B -factory environment, the branching fractions need to be normalised with respect to measurements performed at BABAR and Belle, until the advent of Belle II. This prospective study therefore is split into two periods: a first one based on the assumption of new results from LHCb Run1+Run2 only, and a second one using the complete set of LHCb and Belle II results. The corresponding inputs are gathered in Appendix C. We use the reference scenario described in Table 11 for the central values, so that we can guarantee the self-consistency of the inputs and we avoid reducing the uncertainties artificially because of barely compatible measurements (which would occur if we used the

Fig. 12 Two-dimensional constraints on the real and imaginary parts of hadronic ratios, respectively from *left to right* and from *top to bottom*: N^{0+}/T^{+-} , P_{EW}^C/P_{EW} , P_{EW}^C/P^{+-} , P_{EW}^C/T^{+-} , P^{+-}/P_{EW} , P_{EW}/T^{+-} , P^{+-}/T^{+-} and T_C^{00}/T^{+-} . The *red crosses and dots* indicate our predictions based on QCD factorisation. No prediction is given for the ratio P_{EW}^C/P^{+-} due to numerical instabilities (see text)

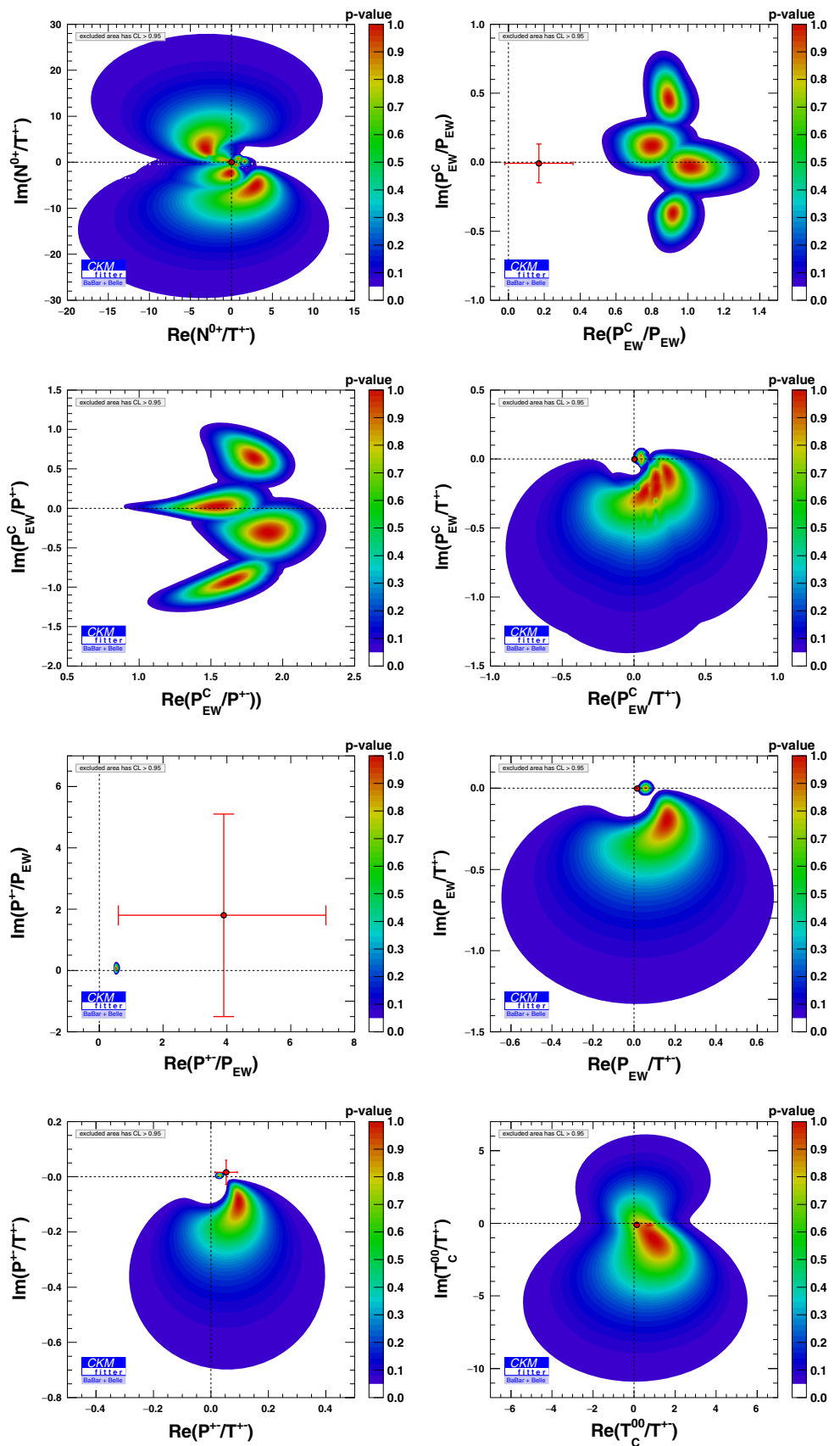


Table 1 68% confidence intervals for the real and imaginary parts of hadronic ratios according to our fit and the corresponding predictions in our implementation of QCD factorisation (QCDF). No prediction is given for the ratio P_{EW}^C/P^{+-} due to numerical instabilities (see text)

Quantity	Fit result	QCDF
$\text{Re} \frac{N^{0+}}{T^{+-}}$	(−5.31, 4.73)	0.011 ± 0.027
$\text{Im} \frac{N^{0+}}{T^{+-}}$	(−9.59, 7.73)	0.003 ± 0.028
$\text{Re} \frac{P_{EW}^C}{P_{EW}}$	(0.69, 1.14)	0.17 ± 0.19
$\text{Im} \frac{P_{EW}^C}{P_{EW}}$	(−0.48, −0.28) \cup (−0.13, 0.22) \cup (0.34, 0.60)	-0.08 ± 0.14
$\text{Re} \frac{P_{EW}^C}{P^{+-}}$	(1.29, 2.08)	–
$\text{Im} \frac{P_{EW}^C}{P^{+-}}$	(−1.09, −0.75) \cup (−0.51, −0.10) \cup (−0.08, 0.16) \cup (0.47, 0.83)	–
$\text{Re} \frac{P_{EW}^C}{T^{+-}}$	(−0.12, 0.34)	0.0027 ± 0.0031
$\text{Im} \frac{P_{EW}^C}{T^{+-}}$	(−0.42, 0.05)	$-0.0015^{+0.0024}_{-0.0025}$
$\text{Re} \frac{P^{+-}}{P_{EW}}$	(0.49, 0.56)	$3.9^{+3.2}_{-3.3}$
$\text{Im} \frac{P^{+-}}{P_{EW}}$	(−0.03, 0.16)	1.8 ± 3.3
$\text{Re} \frac{P_{EW}}{T^{+-}}$	(0.0, 0.25)	$0.0154^{+0.0059}_{-0.0060}$
$\text{Im} \frac{P_{EW}}{T^{+-}}$	(−0.40, −0.09) \cup (−0.02, 0.02)	$-0.0014^{+0.0023}_{-0.0022}$
$\text{Re} \frac{P^{+-}}{T^{+-}}$	(0.023, 0.140)	0.053 ± 0.039
$\text{Im} \frac{P^{+-}}{T^{+-}}$	(−0.20, −0.04) \cup (0.0, 0.01)	0.016 ± 0.044
$\text{Re} \frac{T_C^{00}}{T^{+-}}$	(−0.26, 2.24)	0.13 ± 0.17
$\text{Im} \frac{T_C^{00}}{T^{+-}}$	(−3.28, 0.74)	-0.11 ± 0.15

central values of the current data and rescaled the uncertainties). The expected uncertainties, obtained from the extrapolations discussed previously, are described in Table 12.

The blue area in Fig. 13 illustrates the potential for the first step of our prospective study (B -factories and LHCb Run1 + Run2). For the input values used in the prospective, the modulus of the P^{+-}/T^{+-} ratio will be constrained with a relative 10% accuracy, and its complex phase will be constrained within 3 degrees (we discuss 68% C.L. ranges in the following, whereas Fig. 13 shows 95% C.L. regions). Slightly tighter upper bounds on the $|T_C^{00}/T^{+-}|$ and $|N^{0+}/T^{+-}|$ ratios may be set, albeit the relative phases of these ratios will remain very poorly constrained. Assuming that the electroweak penguin is in agreement with the CPS/GPSZ prediction, its modulus will be constrained within 45% and its phase within 14 degrees.

The addition of results from the Belle II experiment corresponds to the second step of this prospective study. As

illustrated by the green area in Fig. 13, the uncertainties on the modulus and phase of the P^{+-}/T^{+-} ratio will decrease by factors of 1.4 and 2.5, respectively. Owing to the addition of precision measurements by Belle II of the $B^0 \rightarrow K^{*0}\pi^0$ Dalitz-plot parameters from the amplitude analysis of the $B^0 \rightarrow K^+\pi^-\pi^0$ modes, the T_C^{00}/T^{+-} ratio can be constrained within a 22% uncertainty for its modulus, and within 10 degrees for its phase. Similarly, the uncertainties on the modulus and phase of the $P_{EW}/T_{3/2}$ ratio will decrease by factors 2.7 and 2.9, respectively. Concerning the colour-suppressed electroweak penguin, for which only a mild upper bound on its modulus was achievable within the first step of the prospective, can now be measured within a 22% uncertainty for its modulus, and within 8 degrees for its phase. Finally, the less stringent constraint will be achieved for the annihilation parameter. While its modulus can nevertheless be constrained between 0.3 and 1.5, the phase of this ratio may remain unconstrained in value, with just the sign of the

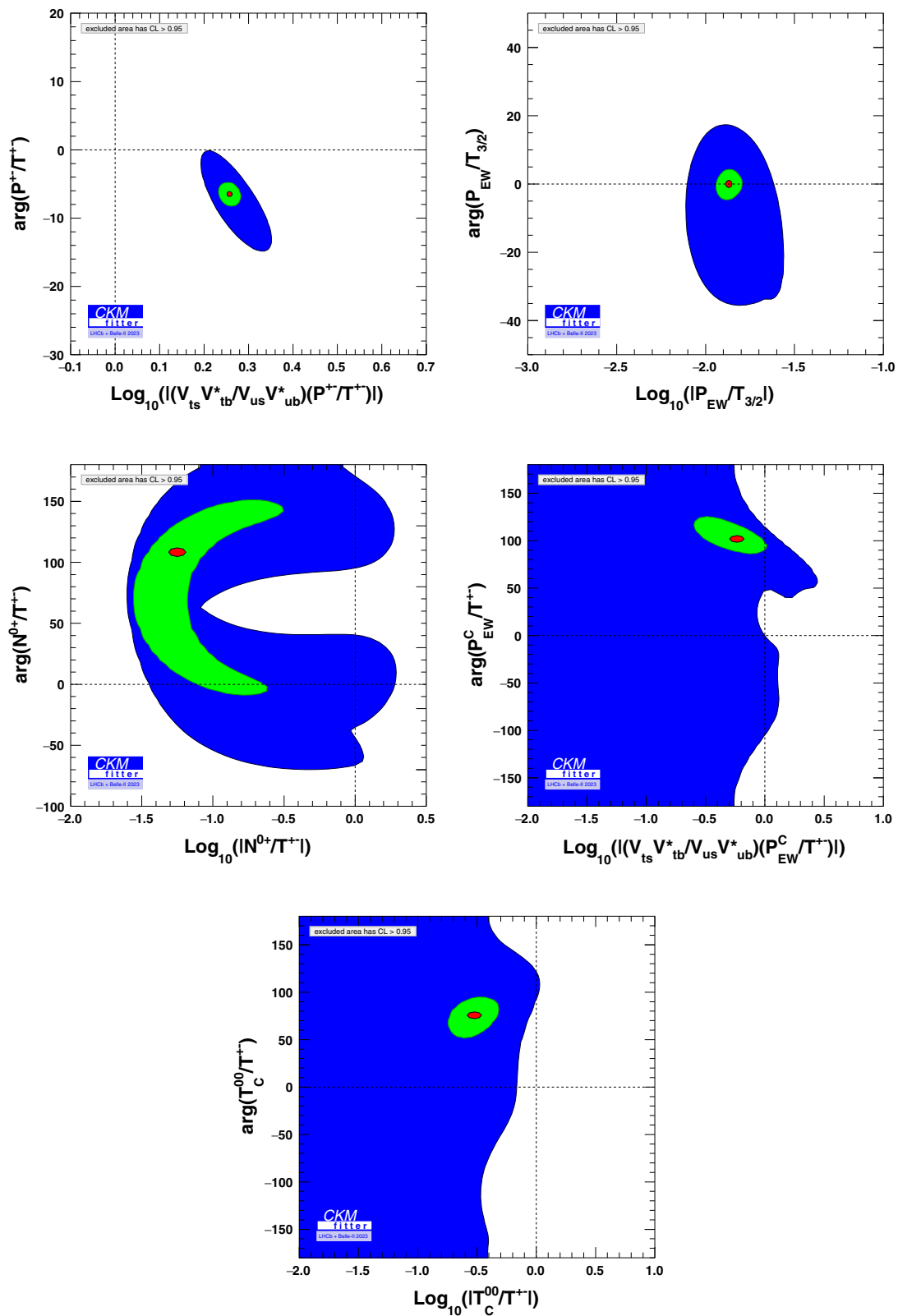


Fig. 13 The expected two-dimensional constraints on the moduli and phases of various ratios of hadronic parameters, using inputs from the first step of the prospective study, based on results from the *B*-factories and expected sensitivities for LHCb Run1 + Run2 (blue area); and using inputs from the second step of the prospective study, based on the com-

plete set of results from LHCb and Belle II (green area). The red spots in the figures represent the generation values obtained from Table 11. From top to bottom and left to right, the hadronic ratios are: P^{+-}/T^{+-} , $P_{EW}/T_{3/2}$, N^{0+}/T^{+-} , P_{EW}^C/T^{+-} , and T_C^{00}/T^{+-} , respectively

phase being resolved. We add that one can also expect Belle II measurements for $B^+ \rightarrow K^+\pi^0\pi^0$ and $B^0 \rightarrow K_S\pi^0\pi^0$, however, with larger uncertainties, so that we have not taken into account these decays.

In total, precise constraints on almost all hadronic parameters in the $B \rightarrow K^*\pi$ system will be achieved using the Dalitz-plot results from the LHCb and Belle II experiments, with a resolution of the current phase ambiguities. These constraints can be compared with various theoretical predictions, proving an important tool for testing models of hadronic contributions to charmless B decays.

7 Conclusion

Non-leptonic B meson decays are very interesting processes both as probes of weak interaction and as tests of our understanding of QCD dynamics. They have been measured extensively at B -factories as well as at the LHCb experiment, but this wealth of data has not been fully exploited yet, especially for the pseudo-scalar–vector modes which are accessible through Dalitz-plot analyses of $B \rightarrow K\pi\pi$ modes. We have focused on the $B \rightarrow K^*\pi$ system which exhibits a large set of observables already measured. Isospin analysis allows us to express this decay in terms of CKM parameters and six complex hadronic amplitudes, but reparametrisation invariance prevents us from extracting simultaneously information on the weak phases and the hadronic amplitudes needed to describe these decays. We have followed two different approaches to exploit this data: either we extracted information on the CKM phase (after setting a condition on some of the hadronic amplitudes), or we determined of hadronic amplitudes (once we set the CKM parameters to their value from the CKM global fit [6–8]).

In the first case, we considered two different strategies. We first reconsidered the CPS/GPSZ strategy proposed in Refs. [64,65], amounting to setting a bound on the electroweak penguin in order to extract an α -like constraint. We used a reference scenario inspired by the current data but with consistent central values and much smaller uncertainties in order to probe the robustness of the CPS/GPSZ method: it turns out that the method is easily biased if the bound on the electroweak penguin is not correct, even by a small amount. Unfortunately, this bound is not very precise from the theoretical point of view, which casts some doubt on the potential of this method to constrain α . We have then considered a more promising alternative, consisting in setting a bound on the annihilation contribution. We observed that we could obtain an interesting stable β -like constraint and we discussed its potential to extract confidence intervals according to the accuracy of the bound used for the annihilation contribution.

In a second stage, we discussed how the data constrain the hadronic amplitudes, assuming the values of the CKM parameters. We performed an average of BABAR and Belle data in order to extract constraints on various ratios of hadronic amplitudes, with the issue that some of these data contain several solutions to be combined in order to obtain a single set of inputs for the Dalitz-plot observables. The ratio P^{+-}/T^{+-} is not very well constrained and exhibits two distinct preferred solutions, but it is not large and supports the expect penguin suppression. On the other hand, colour or electroweak suppression does not seem to hold, as illustrated by $|P_{EW}/P^{+-}|$ (around 2), $|P_{EW}^C/P_{EW}|$ (around 1) or $|T_C^{00}/T^{+-}|$ (mildly favouring values around 1). We, however, recall that some of these conclusions are very dependent on the BABAR measurement on $\varphi^{00,+}$ phase differences measured in $B^0 \rightarrow K^+\pi^+\pi^0$: removing this input turns the ranges into mere upper bounds on these ratios of hadronic amplitudes.

For illustration purposes, we compared these results with typical theoretical expectations. We determined the hadronic amplitudes using an updated implementation of QCD factorisation. A good overall agreement between theory and experiment is found for most of the ratios of hadronic amplitudes, even though the experimental determinations remain often less accurate than the theoretical determinations in most instances. Nevertheless, two quantities still feature interesting properties. The ratio P^{+-}/P_{EW} could provide interesting constraints on the models used to describe power-suppressed contributions in QCD factorisation, keeping in mind the (precise) experimental determination of this ratio relies strongly on the $\varphi^{00,+}$ phases measured by BABAR, as discussed in the previous paragraph. The ratio P_{EW}^C/P_{EW} is determined with similar accuracies theoretically and experimentally, but the two determinations are not in good agreement, suggesting that this quantity could also be used to constrain QCD factorisation parameters.

Finally, we performed prospective studies, considering two successive stages based first on LHCb data from Run1 and Run2, then on the additional input from Belle II. Using our reference scenario and extrapolating the uncertainties of the measurements at both stages, we determined the confidence regions for the moduli and phases of the ratios of hadronic amplitudes. The first stage (LHCb only) would correspond to a significant improvement for P^{+-}/T^{+-} and $P_{EW}/T_{3/2}$, whereas the second stage (LHCb+Belle II) would yield tight constraints on N^{0+}/T^{+-} , P_{EW}^C/T^{+-} and T_C^{00}/T^{+-} .

Non-leptonic B -meson decays remain an important theoretical challenge, and any contender should be able to explain not only the pseudo-scalar–pseudo-scalar modes but also the pseudo-scalar–vector modes. Unfortunately, the current data do not permit such extensive tests, even though they hint at potential discrepancies with theoretical expectations con-

cerning the hierarchies of hadronic amplitudes. However, our study suggests that a more thorough analysis of $B \rightarrow K\pi\pi$ Dalitz plots from LHCb and Belle II could allow for a precise determination of the hadronic amplitudes involved in $B \rightarrow K^*\pi$ decays thanks to the isobar approximation for three-body amplitudes. This will definitely shed some light on the complicated dynamics of weak and strong interaction at work in pseudo-scalar-vector modes, and it will provide important tests of our understanding of non-leptonic B -meson decays.

Acknowledgements We would like to thank all our collaborators from the CKMfitter group for useful discussions, and Reina Camacho Toro for her collaboration on this project at an early stage. This project has received funding from the European Union Horizon 2020 research and innovation programme under the Grant agreements No. 690575, No. 674896 and No. 692194. SDG acknowledges partial support from Contract FPA2014-61478-EXP.

Open Access This article is distributed under the terms of the Creative Commons Attribution 4.0 International License (<http://creativecommons.org/licenses/by/4.0/>), which permits unrestricted use, distribution, and reproduction in any medium, provided you give appropriate credit to the original author(s) and the source, provide a link to the Creative Commons license, and indicate if changes were made. Funded by SCOAP³.

Appendix A: Current experimental inputs

The full set real-valued physical observables, derived from the experimental inputs from BABAR and Belle, is described in the following sections. The errors and correlation matrices include both statistical and systematic uncertainties.

Appendix A.1: BABAR results

In this section, we describe the set of experimental inputs from the BABAR experiment.

Table 2 Central values and total (statistical and systematic) correlation matrix for the global (top) and local (bottom, $\Delta\text{NLL} = 0.16$) minimum solutions for the BABAR $B^0 \rightarrow K_S^0\pi^+\pi^-$ analysis

$B^0 \rightarrow K_S^0\pi^+\pi^-$	Global min	$\text{Re} \left[\frac{q}{p} \frac{\overline{A}(K^{*-}\pi^+)}{A(K^{*+}\pi^-)} \right]$	$\text{Im} \left[\frac{q}{p} \frac{\overline{A}(K^{*-}\pi^+)}{A(K^{*+}\pi^-)} \right]$	$\mathcal{B}(K^{*+}\pi^-)$
$\text{Re} \left[\frac{q}{p} \frac{\overline{A}(K^{*-}\pi^+)}{A(K^{*+}\pi^-)} \right]$	0.428 ± 0.473	1.00	0.90	0.02
$\text{Im} \left[\frac{q}{p} \frac{\overline{A}(K^{*-}\pi^+)}{A(K^{*+}\pi^-)} \right]$	-0.690 ± 0.302		1.00	-0.06
$\mathcal{B}(K^{*+}\pi^-)(\times 10^{-6})$	8.290 ± 1.189			1.00
$B^0 \rightarrow K_S^0\pi^+\pi^-$	Local min ($\Delta\text{NLL} = 0.16$)	$\text{Re} \left[\frac{q}{p} \frac{\overline{A}(K^{*-}\pi^+)}{A(K^{*+}\pi^-)} \right]$	$\text{Im} \left[\frac{q}{p} \frac{\overline{A}(K^{*-}\pi^+)}{A(K^{*+}\pi^-)} \right]$	$\mathcal{B}(K^{*+}\pi^-)$
$\text{Re} \left[\frac{q}{p} \frac{\overline{A}(K^{*-}\pi^+)}{A(K^{*+}\pi^-)} \right]$	-0.819 ± 0.116	1.00	-0.19	-0.15
$\text{Im} \left[\frac{q}{p} \frac{\overline{A}(K^{*-}\pi^+)}{A(K^{*+}\pi^-)} \right]$	-0.049 ± 0.494		1.00	-0.01
$\mathcal{B}(K^{*+}\pi^-)(\times 10^{-6})$	8.290 ± 1.189			1.00

Table 3 Central values of the observables for the BABAR $B^+ \rightarrow K^+\pi^-\pi^+$ analysis

$B^+ \rightarrow K^+\pi^-\pi^+$	Value
$\left \frac{\overline{A}(K^{*0}\pi^-)}{A(K^{*0}\pi^+)} \right $	1.033 ± 0.047
$\mathcal{B}(K^{*0}\pi^+)(\times 10^{-6})$	10.800 ± 1.389

- $B^0 \rightarrow K_S^0\pi^+\pi^-$ [38]. Two almost degenerate solutions were found differing only by 0.16 negative-log-likelihood (ΔNLL) units. The central values and correlation matrix of the measured observables for both solutions are shown in Table 2.
- $B^+ \rightarrow K^+\pi^-\pi^+$ [39]. The central values of the observables for this analysis are shown in Table 3. A linear correlation of 2% was found between $\left| \frac{\overline{A}(K^{*0}\pi^-)}{A(K^{*0}\pi^+)} \right|$ and $\mathcal{B}(K^{*0}\pi^+)$.
- $B^0 \rightarrow K^+\pi^-\pi^0$ [40]. The central values and correlation matrix of the measured observables for this analysis are shown in Table 4.
- $B^+ \rightarrow K_S^0\pi^+\pi^0$ [41]. The central values and correlation matrix of the measured observables for this analysis are shown in Table 5.
- $B^+ \rightarrow K^{*+}(892)\pi^0$ quasi-two-body contribution to the $B^+ \rightarrow K^+\pi^0\pi^0$ final state [42]. The measured branching ratio and CP asymmetry are shown in Table 6 and they are used as uncorrelated inputs.

Appendix A.2: Belle results

In this section, we describe the set of experimental inputs from the Belle experiment.

Table 4 Central values and total (statistical and systematic) correlation matrix for observables from the BABAR $B^0 \rightarrow K^+\pi^-\pi^0$ analysis

$B^0 \rightarrow K^+\pi^-\pi^0$	Value	$\left \frac{\overline{A}(K^{*-}\pi^+)}{A(K^{*+}\pi^-)} \right $	$\text{Re} \left[\frac{A(K^{*0}\pi^0)}{A(K^{*+}\pi^-)} \right]$	$\text{Im} \left[\frac{A(K^{*0}\pi^0)}{A(K^{*+}\pi^-)} \right]$	$\text{Re} \left[\frac{\overline{A}(K^{*0}\pi^0)}{A(K^{*-}\pi^+)} \right]$	$\text{Re} \left[\frac{\overline{A}(K^{*0}\pi^0)}{A(K^{*-}\pi^+)} \right]$	$\mathcal{B}(K^{*0}\pi^0)$
$\left \frac{\overline{A}(K^{*-}\pi^+)}{A(K^{*+}\pi^-)} \right $	0.742 ± 0.091	1.00	0.00	0.03	-0.22	-0.11	-0.06
$\text{Re} \left[\frac{A(K^{*0}\pi^0)}{A(K^{*+}\pi^-)} \right]$	0.562 ± 0.148		1.00	0.68	0.33	-0.01	0.44
$\text{Im} \left[\frac{A(K^{*0}\pi^0)}{A(K^{*+}\pi^-)} \right]$	-0.227 ± 0.296			1.00	-0.07	0.00	-0.13
$\text{Re} \left[\frac{\overline{A}(K^{*0}\pi^0)}{A(K^{*-}\pi^+)} \right]$	0.701 ± 0.126				1.00	0.25	0.55
$\text{Im} \left[\frac{\overline{A}(K^{*0}\pi^0)}{A(K^{*-}\pi^+)} \right]$	-0.049 ± 0.376					1.00	-0.02
$\mathcal{B}(K^{*0}\pi^0)(\times 10^{-6})$	3.300 ± 0.640						1.00

Table 5 Central values and total (statistical and systematic) correlation matrix for observables from the BABAR $B^+ \rightarrow K_S^0\pi^+\pi^0$ analysis

$B^+ \rightarrow K_S^0\pi^+\pi^0$	Value	$\left \frac{\overline{A}(K^{*-}\pi^0)}{A(K^{*+}\pi^0)} \right $	$\text{Re} \left[\frac{A(K^{*+}\pi^0)}{A(K^{*0}\pi^+)} \right]$	$\text{Im} \left[\frac{A(K^{*+}\pi^0)}{A(K^{*0}\pi^+)} \right]$	$\text{Re} \left[\frac{\overline{A}(K^{*-}\pi^0)}{A(K^{*0}\pi^+)} \right]$	$\text{Im} \left[\frac{\overline{A}(K^{*-}\pi^0)}{A(K^{*0}\pi^+)} \right]$	$\mathcal{B}(K^{*+}\pi^0)$
$\left \frac{\overline{A}(K^{*-}\pi^0)}{A(K^{*+}\pi^0)} \right $	0.533 ± 1.403	1.00	-0.26	0.01	-0.70	-0.22	-0.16
$\text{Re} \left[\frac{A(K^{*+}\pi^0)}{A(K^{*0}\pi^+)} \right]$	1.415 ± 6.952		1.00	-0.23	0.12	-0.51	0.90
$\text{Im} \left[\frac{A(K^{*+}\pi^0)}{A(K^{*0}\pi^+)} \right]$	-0.189 ± 3.646			1.00	-0.39	0.23	-0.28
$\text{Re} \left[\frac{\overline{A}(K^{*-}\pi^0)}{A(K^{*0}\pi^+)} \right]$	-0.106 ± 2.687				1.00	0.23	0.03
$\text{Im} \left[\frac{\overline{A}(K^{*-}\pi^0)}{A(K^{*0}\pi^+)} \right]$	-0.851 ± 4.278					1.00	-0.82
$\mathcal{B}(K^{*+}\pi^0)(\times 10^{-6})$	9.200 ± 1.480						1.00

Table 6 Central values of the observables from the BABAR analysis of $B^+ \rightarrow K^{*+}(892)\pi^0$ quasi-two-body contribution to the $B^+ \rightarrow K^+\pi^0\pi^0$

$B^+ \rightarrow K^{*+}\pi^0$ in $B^+ \rightarrow K^+\pi^0\pi^0$	Value
$\mathcal{B}(K^{*+}\pi^0)$	$(8.2 \pm 1.5 \pm 1.1) \times 10^{-6}$
$A_{\text{CP}}(K^{*+}\pi^0)$	$-0.06 \pm 0.24 \pm 0.04$

- $B^0 \rightarrow K_S^0\pi^+\pi^-$ [44]. Two solutions were found differing by 7.5 ΔNLL . The central values and correlation matrix of the measured observables for both solutions are shown in Table 7.
- $B^+ \rightarrow K^+\pi^-\pi^+$ [43]. The central values of the observables for this analysis are shown in Table 8. A nearly vanishing correlation was found between $\left| \frac{\overline{A}(K^{*0}\pi^-)}{A(K^{*0}\pi^+)} \right|$ and $\mathcal{B}(K^{*0}\pi^+)$.

Appendix A.3: Combined BABAR and Belle results

The BABAR and Belle results for the $B^0 \rightarrow K_S^0\pi^+\pi^-$ and $B^+ \rightarrow K^+\pi^-\pi^+$ analyses shown previously have been combined in the usual way for sets of independent measure-

ments. The combination for the $B^+ \rightarrow K^+\pi^-\pi^+$ mode is straightforward as the results exhibit only one solution, as shown in Fig. 14. The resulting central values are shown in Table 9. A vanishing linear correlation is found between $\left| \frac{\overline{A}(K^{*0}\pi^-)}{A(K^{*0}\pi^+)} \right|$ and $\mathcal{B}(K^{*0}\pi^+)$.

The combination of the BABAR and Belle measurements for the $B^0 \rightarrow K_S^0\pi^+\pi^-$ mode is more complicated as the results feature several solutions which are relatively close in units of ΔNLL . In order to combine these measurements we proceed as follows:

- We combine each solution of the BABAR analysis with each one of the Belle results.
- In the goodness of fit of the combination (χ_{min}^2), we add the ΔNLL of each BABAR and Belle solution. In the case of the global minimum the corresponding ΔNLL is zero.
- Finally, we take the envelope of the four combinations as the final result.

We find the following χ_{min}^2 for the four combinations: 1.1, 8.7, 9.5 and 98.3. As the closest combination from the global minimum differs by 7.6 units in χ_{min}^2 , we have decided

Table 7 Central values and total (statistical and systematic) correlation matrix for the global (top) and local solution (bottom, $\Delta\text{NLL} = 7.5$) minimum solutions of the observables from the Belle $B^0 \rightarrow K_S^0 \pi^+ \pi^-$ analysis

$B^0 \rightarrow K_S^0 \pi^+ \pi^-$	Global min	$\text{Re} \left[\frac{q}{p} \frac{\bar{A}(K^{*-} \pi^+)}{A(K^{*+} \pi^-)} \right]$	$\text{Im} \left[\frac{q}{p} \frac{\bar{A}(K^{*-} \pi^+)}{A(K^{*+} \pi^-)} \right]$	$\mathcal{B}(K^{*+} \pi^-)$
$\text{Re} \left[\frac{q}{p} \frac{\bar{A}(K^{*-} \pi^+)}{A(K^{*+} \pi^-)} \right]$	0.790 ± 0.145	1.00	0.62	-0.04
$\text{Im} \left[\frac{q}{p} \frac{\bar{A}(K^{*-} \pi^+)}{A(K^{*+} \pi^-)} \right]$	-0.206 ± 0.398		1.00	0.00
$\mathcal{B}(K^{*+} \pi^-) (\times 10^{-6})$	8.400 ± 1.449			1.00
$B^0 \rightarrow K_S^0 \pi^+ \pi^-$	Local min ($\Delta\text{NLL} = 7.5$)	$\text{Re} \left[\frac{q}{p} \frac{\bar{A}(K^{*-} \pi^+)}{A(K^{*+} \pi^-)} \right]$	$\text{Im} \left[\frac{q}{p} \frac{\bar{A}(K^{*-} \pi^+)}{A(K^{*+} \pi^-)} \right]$	$\mathcal{B}(K^{*+} \pi^-)$
$\text{Re} \left[\frac{q}{p} \frac{\bar{A}(K^{*-} \pi^+)}{A(K^{*+} \pi^-)} \right]$	0.808 ± 0.110	1.00	0.01	-0.06
$\text{Im} \left[\frac{q}{p} \frac{\bar{A}(K^{*-} \pi^+)}{A(K^{*+} \pi^-)} \right]$	0.010 ± 0.439		1.00	0.00
$\mathcal{B}(K^{*+} \pi^-) (\times 10^{-6})$	8.400 ± 1.449			1.00

Table 8 Central values of the observables from the Belle $B^+ \rightarrow K^+ \pi^- \pi^+$ analysis

$B^+ \rightarrow K^+ \pi^- \pi^+$	Value
$\left \frac{\bar{A}(K^{*0} \pi^-)}{A(K^{*0} \pi^+)} \right $	0.861 ± 0.059
$\mathcal{B}(K^{*0} \pi^+) (\times 10^{-6})$	9.670 ± 1.061

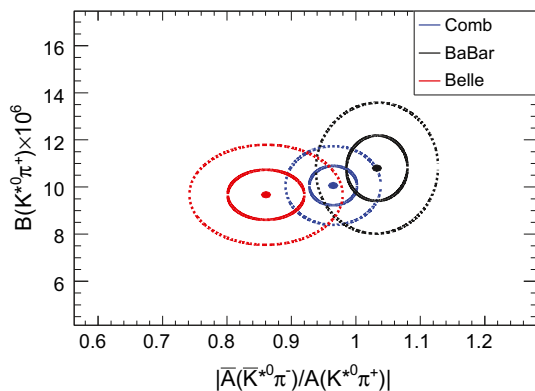


Fig. 14 Contours at 1 (solid) and 2 (dotted) σ in the $\left| \frac{\bar{A}(K^{*0} \pi^-)}{A(K^{*0} \pi^+)} \right|$ vs. $\mathcal{B}(K^{*0} \pi^+)$ plane for the BABAR (black) and Belle (red) results, as well as the combination (blue)

to focus on the global minimum for the phenomenological analysis. The combination for this global minimum is shown in Fig. 15. The resulting central values and covariance matrix are shown in Table 9.

These combined results for the $B^0 \rightarrow K_S^0 \pi^+ \pi^-$ and $B^+ \rightarrow K^+ \pi^- \pi^+$ modes are used with the BABAR results for the $B^0 \rightarrow K^+ \pi^- \pi^0$ and $B^+ \rightarrow K_S^0 \pi^+ \pi^0$ as inputs for the phenomenological analysis using the current experimental measurements.

Appendix B: Two-body non-leptonic amplitudes in QCD factorisation

We compute the $B \rightarrow K^* \pi$ amplitudes in the framework of QCD factorisation, using the results of Ref. [16]. We take the semileptonic $B \rightarrow \pi$ and $B \rightarrow K \pi$ form factors from computations based on light-cone sum rules [75,76]. The parameters for the light-meson distribution amplitudes that enter hard-scattering contributions are consistently taken from the last two references. On the other hand the first inverse moment of the B -meson distribution amplitude λ_B is taken from Ref. [77]. Quark masses are taken from the review by the FLAG group [78]. Our updated inputs are summarised in Table 10.

We stress that the calculations of Ref. [16] correspond to Next-to-Leading Order (NLO). Since then, some NNLO contributions have been computed [57,79–82], that we neglect in view of the sizeable uncertainties on the input parameters: this is sufficient for our illustrative purposes (see Sect. 5.3).

Appendix C: Reference scenario and prospective studies

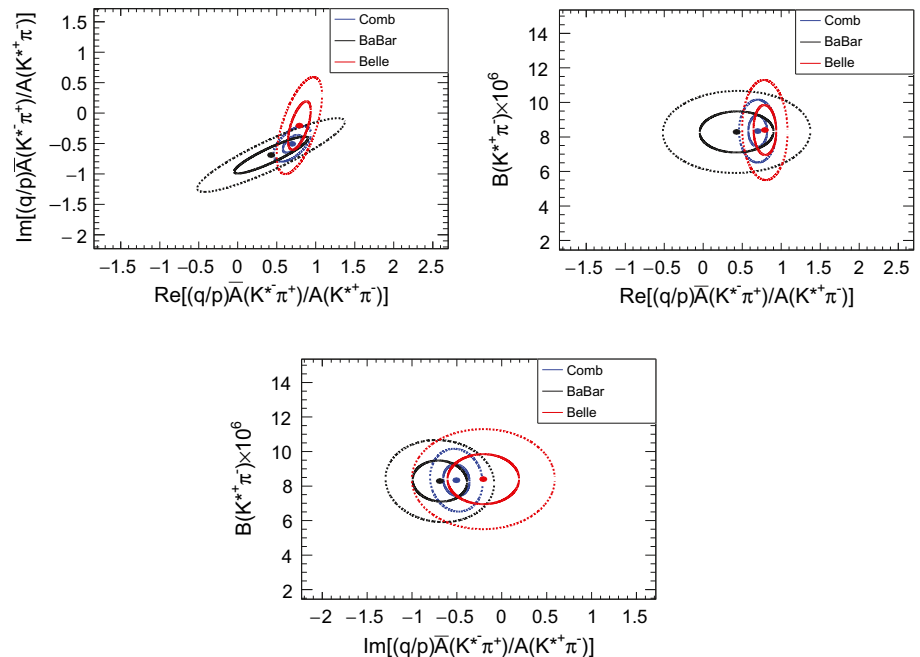
Some of the experimental results collected in Appendix A are affected by large uncertainties, and the central values are not always fully consistent with SM expectations. This is not a problem when we want to extract values of the hadronic parameters from the data, but it makes rather unclear the discussion of the accuracy of specific models (say, for the extraction of weak angles) or the prospective studies assuming improved experimental measurements; see Sects. 4 and 6.

For this reason, we design a reference scenario described in Table 11. The values on hadronic parameters are chosen to reproduce the current best averages of branching fractions and CP asymmetries in $B \rightarrow K^* \pi$ roughly. As most observable phase differences among these modes are

Table 9 Central values of the observables from the $B^+ \rightarrow K^+\pi^-\pi^+$ (top) and $B^0 \rightarrow K_S^0\pi^+\pi^-$ (bottom) analysis obtained by combining BABAR and Belle results

$B^+ \rightarrow K^+\pi^-\pi^+$		Value			
$\left \frac{\bar{A}(K^0\pi^-)}{A(K^0\pi^+)} \right $		0.965 ± 0.037			
$\mathcal{B}(K^*0\pi^+)(\times 10^{-6})$		10.062 ± 0.835			
$B^0 \rightarrow K_S^0\pi^+\pi^-$		Value	$\text{Re} \left[\frac{q}{p} \frac{\bar{A}(K^{*0}\pi^+)}{A(K^{*0}\pi^-)} \right]$	$\text{Im} \left[\frac{q}{p} \frac{\bar{A}(K^{*0}\pi^+)}{A(K^{*0}\pi^-)} \right]$	$\mathcal{B}(K^{*+}\pi^-)$
$\text{Re} \left[\frac{q}{p} \frac{\bar{A}(K^{*0}\pi^+)}{A(K^{*0}\pi^-)} \right]$	0.698 ± 0.120	1.00	0.58	-0.01	
$\text{Im} \left[\frac{q}{p} \frac{\bar{A}(K^{*0}\pi^+)}{A(K^{*0}\pi^-)} \right]$	-0.506 ± 0.146		1.00	-0.09	
$\mathcal{B}(K^{*+}\pi^-)(\times 10^{-6})$	8.340 ± 0.910			1.00	

Fig. 15 Contours at 1 (solid) and 2 (dotted) σ in the $\text{Re} \left[\frac{q}{p} \frac{\bar{A}(K^{*+}\pi^-)}{A(K^{*+}\pi^+)} \right]$ vs. $\text{Im} \left[\frac{q}{p} \frac{\bar{A}(K^{*+}\pi^-)}{A(K^{*+}\pi^+)} \right]$ (upper row, left), $\text{Re} \left[\frac{q}{p} \frac{\bar{A}(K^{*+}\pi^-)}{A(K^{*+}\pi^+)} \right]$ vs. $\mathcal{B}(K^{*+}\pi^-)$ (upper row, right) and $\text{Im} \left[\frac{q}{p} \frac{\bar{A}(K^{*+}\pi^-)}{A(K^{*+}\pi^+)} \right]$ vs. $\mathcal{B}(K^{*+}\pi^-)$ (lower row) planes for the BABAR (black) and Belle (red) results, as well as the combination (blue)



poorly constrained by the results currently available, we do not attempt at reproducing their central values and we use the values resulting from the hadronic parameters. The hadronic amplitudes are constrained to respect the naive assumptions: $|P_{EW}/T_{3/2}| \simeq 1.35\%$, $|P_{EW}^C| < |P_{EW}|$ and $|T_C^{00}| < |T^{+-}|$. The best values of the hadronic parameters yield the values of branching ratios and CP asymmetries gathered in Table 11. As can be seen, the overall agreement is fair, but it is not good for all observables. Indeed, as discussed in Sect. 5, the current data do not favour all the hadronic hierarchies that we have imposed to obtain our reference scenario in Table 11.

For the studies of different methods to extract CKM parameters described in Sect. 4, we fit the values of hadronic parameters by assigning small, arbitrary, uncertainties to the physical observables: $\pm 5\%$ for branching ratios, $\pm 0.5\%$ for CP asymmetries, and $\pm 5^\circ$ for interference phases.

For the prospective studies described in Sect. 6, we estimate future experimental uncertainties at two different stages. We first consider a list of expected measurements

from LHCb, using the combined Run1 and Run2 data. We then reassess the expected results including Belle II measurements. Our method to project uncertainties in the two stages is based on the statistical scaling of data samples ($1/\sqrt{N_{\text{evts}}}$), corrected for additional factors due to particular detector performances and analysis technique features, as described below.

LHCb Run1 and Run2 data will significantly increase the statistics mainly for the fully charged final states $B^0 \rightarrow K_S^0(\rightarrow \pi^+\pi^-)\pi^+\pi^-$ and $B^+ \rightarrow K^+\pi^-\pi^+$, with an expected increase of about 3 and 40, respectively [70, 71]. For these modes, we assume a signal-to-background ratio similar to the ones measured at B factories (this may represent an underestimation of the potential sensitivity of LHCb data, but this assumption has a very minor impact on the results of our prospective study). The statistical scaling factor thus defined can be applied as such to direct CP asymmetries, but some additional aspects must be considered in the scaling of uncertainties for other observables. For time-dependent

Table 10 Input values for the hadronic parameters that enter QCD factorisation predictions: moments of the distribution amplitudes for mesons, decay constants, form factors and quark masses. Dimensionful

Input	Value	Input	Value
$\alpha_1(K^*)$	$0.06 \pm 0 \pm 0.04$	$\alpha_1(K^*, \perp)$	$0.04 \pm 0 \pm 0.03$
$\alpha_2(K^*)$	$0.16 \pm 0 \pm 0.09$	$\alpha_2(K^*, \perp)$	$0.10 \pm 0 \pm 0.08$
$f_{\perp}(K^*)$	$0.159 \pm 0 \pm 0.006$	$A_0[B \rightarrow K^*](0)$	$0.356 \pm 0 \pm 0.046$
$\alpha_2(\pi)$	$0.062 \pm 0 \pm 0.054$	$F_0[B \rightarrow \pi](0)$	$0.258 \pm 0 \pm 0.031$
λ_B	$0.460 \pm 0 \pm 0.110$	\bar{m}_b	4.17
\bar{m}_s	$0.0939 \pm 0 \pm 0.0011$	m_q/m_s	~ 0

quantities are in GeV. The ± 0 in second position means that all uncertainties are considered as coming from a theoretical origin and they are treated according to the Rfit approach. See the text for references

Table 11 Values chosen for our reference scenario. The values on hadronic parameters (left columns) are chosen to roughly reproduce the reference values of branching fractions (in units of 10^{-6}) and CP asymmetries in $B \rightarrow K^*\pi$ (right columns). The reference input values

come from the current HFLAV averages [66], except for $A_{CP}(B^+ \rightarrow K^{*+}\pi^0)$, where the value is taken from Ref. [41]. The values of the hadronic parameters yield the branching ratios and CP asymmetries of the last column

Hadronic amplitudes	Magnitude	Phase ($^\circ$)	Observable	Measurement	Value
T^{+-}	2.540	0.0	$\mathcal{B}(B^0 \rightarrow K^{*+}\pi^-)$	8.4 ± 0.8	7.1
T_C^{00}	0.762	75.8	$\mathcal{B}(B^0 \rightarrow K^{*0}\pi^0)$	3.3 ± 0.6	1.6
N^{0+}	0.143	108.4	$\mathcal{B}(B^+ \rightarrow K^{*+}\pi^0)$	8.2 ± 1.8	8.5
P^{+-}	0.091	-6.5	$\mathcal{B}(B^+ \rightarrow K^{*0}\pi^+)$	$10.1^{+0.8}_{-0.9}$	10.9
P_{EW}	0.038	15.2	$A_{CP}(B^0 \rightarrow K^{*+}\pi^-)$	-0.23 ± 0.06	-0.129
P_{EW}^C	0.029	101.9	$A_{CP}(B^0 \rightarrow K^{*0}\pi^0)$	-0.15 ± 0.13	+0.465
$\left \frac{V_{ts} V_{tb}^* P^{+-}}{V_{us} V_{ub}^* T^{+-}} \right $	1.809		$A_{CP}(B^+ \rightarrow K^{*+}\pi^0)$	-0.39 ± 0.12	-0.355
$ T_C^{00}/T^{+-} $	0.300		$A_{CP}(B^+ \rightarrow K^{*0}\pi^+)$	$+0.038 \pm 0.042$	+0.039
$ N^{0+}/T_C^{00} $	0.187				
$ P_{EW}/P^{+-} $	0.421				
$ P_{EW}/(T^{+-} + T_C^{00}) /R$	1.009				
$ P_{EW}^C/P_{EW} $	0.762				

CP asymmetries, the difference in flavour-tagging performances (the effective tagging efficiency Q) should be taken into account. In the B -factory environment, a quality factor $Q_{B\text{-factories}} \sim 30$ [73, 74] was achieved, while for LHCb a smaller value is used ($Q_{LHCb} \sim 3$ [72]), which entails an additional factor $(Q_{B\text{-factories}}/Q_{LHCb})^{1/2} \sim 3.2$ in the scaling of uncertainties. For branching ratios, LHCb is not able to directly count the number of B mesons produced, and it is necessary to resort to a normalisation using final states for which the branching ratio has been measured elsewhere (mainly at B -factories). This additional source of uncertainty is taken into account in the projection of the error. Finally, in our prospective studies, we adopt the pessimistic view of neglecting potential measurements from LHCb for modes with π^0 mesons in the final state (e.g., $B^0 \rightarrow K^+\pi^-\pi^0$ and

$B^+ \rightarrow K_S^0\pi^+\pi^0$), as it is difficult to anticipate the evolution in the performances for π^0 reconstruction and phase space resolution.

Belle II [69] expects to surpass by a factor of ~ 50 the total statistics collected by the B -factories. As the experimental environments will be very similar, we just scale the current uncertainties by this statistical factor.

Starting from the statistical uncertainties from Babar and scaling them according to the above procedure, we obtain our projections of uncertainties on physical observables, shown in Table 12, where the current uncertainties are compared with the projected ones for the first (B -factories combined with LHCb Run1 and Run2) and second (adding Belle II) stages described previously.

Table 12 Prospective scenarios for statistical uncertainties on the $B \rightarrow K^* \pi$ observables. The extrapolations are based on the current statistical uncertainties from BABAR results. The uncertainties on the branching fractions are given in units of 10^{-6}

Observable	Analysis	Current uncertainty	LHCb (Run1 + Run2)	LHCb + Belle II
$\text{Re} \left[\frac{q}{p} \frac{\overline{A}(K^{*-}\pi^+)}{A(K^{*+}\pi^-)} \right]$	$B^0 \rightarrow K_S^0 \pi^+ \pi^-$	0.11	0.04	0.01
$\text{Im} \left[\frac{q}{p} \frac{\overline{A}(K^{*-}\pi^+)}{A(K^{*+}\pi^-)} \right]$	$B^0 \rightarrow K_S^0 \pi^+ \pi^-$	0.16	0.11	0.02
$\mathcal{B}(K^{*+}\pi^-)$	$B^0 \rightarrow K_S^0 \pi^+ \pi^-$	0.69	0.32	0.09
$\left \frac{\overline{A}(K^{*-}\pi^+)}{A(K^{*+}\pi^-)} \right $	$B^0 \rightarrow K^+ \pi^- \pi^0$	0.06	0.06	0.01
$\text{Re} \left[\frac{A(K^{*0}\pi^0)}{A(K^{*+}\pi^-)} \right]$	$B^0 \rightarrow K^+ \pi^- \pi^0$	0.11	0.11	0.02
$\text{Im} \left[\frac{A(K^{*0}\pi^0)}{A(K^{*+}\pi^-)} \right]$	$B^0 \rightarrow K^+ \pi^- \pi^0$	0.23	0.23	0.03
$\text{Re} \left[\frac{\overline{A}(K^{*0}\pi^0)}{A(K^{*-}\pi^+)} \right]$	$B^0 \rightarrow K^+ \pi^- \pi^0$	0.10	0.10	0.01
$\text{Im} \left[\frac{\overline{A}(K^{*0}\pi^0)}{A(K^{*-}\pi^+)} \right]$	$B^0 \rightarrow K^+ \pi^- \pi^0$	0.30	0.30	0.04
$\mathcal{B}(K^{*0}\pi^0)$	$B^0 \rightarrow K^+ \pi^- \pi^0$	0.35	0.35	0.05
$\left \frac{\overline{A}(K^{*0}\pi^-)}{A(K^{*0}\pi^+)} \right $	$B^+ \rightarrow K^+ \pi^- \pi^+$	0.04	0.005	0.004
$\mathcal{B}(K^{*0}\pi^+)$	$B^+ \rightarrow K^+ \pi^- \pi^+$	0.81	0.50	0.11
$\left \frac{\overline{A}(K^{*-}\pi^0)}{A(K^{*+}\pi^0)} \right $	$B^+ \rightarrow K_S^0 \pi^+ \pi^0$	0.15	0.15	0.02
$\text{Re} \left[\frac{A(K^{*+}\pi^0)}{A(K^{*0}\pi^+)} \right]$	$B^+ \rightarrow K_S^0 \pi^+ \pi^0$	0.16	0.16	0.02
$\text{Im} \left[\frac{A(K^{*+}\pi^0)}{A(K^{*0}\pi^+)} \right]$	$B^+ \rightarrow K_S^0 \pi^+ \pi^0$	0.30	0.30	0.04
$\text{Re} \left[\frac{\overline{A}(K^{*-}\pi^0)}{A(K^{*0}\pi^-)} \right]$	$B^+ \rightarrow K_S^0 \pi^+ \pi^0$	0.21	0.21	0.03
$\text{Im} \left[\frac{\overline{A}(K^{*-}\pi^0)}{A(K^{*0}\pi^-)} \right]$	$B^+ \rightarrow K_S^0 \pi^+ \pi^0$	0.13	0.13	0.02
$\mathcal{B}(K^{*+}\pi^0)$	$B^+ \rightarrow K_S^0 \pi^+ \pi^0$	0.92	0.92	0.13

References

1. A.J. Bevan et al., [BABAR and Belle Collaborations], Eur. Phys. J. C **74**, 3026 (2014). doi:[10.1140/epjc/s10052-014-3026-9](https://doi.org/10.1140/epjc/s10052-014-3026-9). arXiv:[1406.6311](https://arxiv.org/abs/1406.6311) [hep-ex]
2. R. Aaij et al. [LHCb Collaboration], Eur. Phys. J. C **73**(4), 2373 (2013). doi:[10.1140/epjc/s10052-013-2373-2](https://doi.org/10.1140/epjc/s10052-013-2373-2). arXiv:[1208.3355](https://arxiv.org/abs/1208.3355) [hep-ex]
3. N. Cabibbo, Phys. Rev. Lett. **10**, 531 (1963). doi:[10.1103/PhysRevLett.10.531](https://doi.org/10.1103/PhysRevLett.10.531)
4. M. Kobayashi, T. Maskawa, Prog. Theor. Phys. **49**, 652 (1973). doi:[10.1143/PTP.49.652](https://doi.org/10.1143/PTP.49.652)
5. O. Deschamps et al., work in progress
6. J. Charles et al., [CKMfitter Group], Eur. Phys. J. C **41**, 1 (2005). arXiv:[hep-ph/0406184](https://arxiv.org/abs/hep-ph/0406184)
7. Updates and numerical results on the CKMfitter group, <http://ckmfitter.in2p3.fr/>
8. J. Charles et al., Phys. Rev. D **91**(7), 073007 (2015). doi:[10.1103/PhysRevD.91.073007](https://doi.org/10.1103/PhysRevD.91.073007). arXiv:[1501.05013](https://arxiv.org/abs/1501.05013) [hep-ph]
9. P. Koppenburg, S. Descotes-Genon, arXiv:[1702.08834](https://arxiv.org/abs/1702.08834) [hep-ex]
10. J. Charles, S. Descotes-Genon, Z. Ligeti, S. Monteil, M. Papucci, K. Trabelsi, Phys. Rev. D **89**(3), 033016 (2014). doi:[10.1103/PhysRevD.89.033016](https://doi.org/10.1103/PhysRevD.89.033016). arXiv:[1309.2293](https://arxiv.org/abs/1309.2293) [hep-ph]
11. A. Lenz, U. Nierste, J. Charles, S. Descotes-Genon, H. Lacker, S. Monteil, V. Niess, S. T'Jampens, Phys. Rev. D **86**, 033008 (2012). doi:[10.1103/PhysRevD.86.033008](https://doi.org/10.1103/PhysRevD.86.033008). arXiv:[1203.0238](https://arxiv.org/abs/1203.0238) [hep-ph]
12. A. Lenz et al., Phys. Rev. D **83**, 036004 (2011). doi:[10.1103/PhysRevD.83.036004](https://doi.org/10.1103/PhysRevD.83.036004). arXiv:[1008.1593](https://arxiv.org/abs/1008.1593) [hep-ph]
13. O. Deschamps, S. Descotes-Genon, S. Monteil, V. Niess, S. T'Jampens, V. Tisserand, Phys. Rev. D **82**, 073012 (2010). doi:[10.1103/PhysRevD.82.073012](https://doi.org/10.1103/PhysRevD.82.073012). arXiv:[0907.5135](https://arxiv.org/abs/0907.5135) [hep-ph]
14. M. Beneke, G. Buchalla, M. Neubert, C.T. Sachrajda, Phys. Rev. Lett. **83**, 1914 (1999). doi:[10.1103/PhysRevLett.83.1914](https://doi.org/10.1103/PhysRevLett.83.1914). arXiv:[hep-ph/9905312](https://arxiv.org/abs/hep-ph/9905312)
15. M. Beneke, G. Buchalla, M. Neubert, C.T. Sachrajda, Nucl. Phys. B **591**, 313 (2000). doi:[10.1016/S0550-3213\(00\)00559-9](https://doi.org/10.1016/S0550-3213(00)00559-9). arXiv:[hep-ph/0006124](https://arxiv.org/abs/hep-ph/0006124)
16. M. Beneke, M. Neubert, Nucl. Phys. B **675**, 333 (2003). doi:[10.1016/j.nuclphysb.2003.09.026](https://doi.org/10.1016/j.nuclphysb.2003.09.026). arXiv:[hep-ph/0308039](https://arxiv.org/abs/hep-ph/0308039)
17. M. Beneke, J. Rohrer, D. Yang, Nucl. Phys. B **774**, 64 (2007). doi:[10.1016/j.nuclphysb.2007.03.020](https://doi.org/10.1016/j.nuclphysb.2007.03.020). arXiv:[hep-ph/0612290](https://arxiv.org/abs/hep-ph/0612290)
18. H.N. Li, Phys. Rev. D **66**, 094010 (2002). doi:[10.1103/PhysRevD.66.094010](https://doi.org/10.1103/PhysRevD.66.094010). arXiv:[hep-ph/0102013](https://arxiv.org/abs/hep-ph/0102013)
19. H.N. Li, K. Ukai, Phys. Lett. B **555**, 197 (2003). doi:[10.1016/S0370-2693\(03\)00049-2](https://doi.org/10.1016/S0370-2693(03)00049-2). arXiv:[hep-ph/0211272](https://arxiv.org/abs/hep-ph/0211272)
20. H.N. Li, Prog. Part. Nucl. Phys. **51**, 85 (2003). doi:[10.1016/S0146-6410\(03\)90013-5](https://doi.org/10.1016/S0146-6410(03)90013-5). arXiv:[hep-ph/0303116](https://arxiv.org/abs/hep-ph/0303116)
21. A. Ali, G. Kramer, Y. Li, C.D. Lu, Y.L. Shen, W. Wang, Y.M. Wang, Phys. Rev. D **76**, 074018 (2007). doi:[10.1103/PhysRevD.76.074018](https://doi.org/10.1103/PhysRevD.76.074018). arXiv:[hep-ph/0703162](https://arxiv.org/abs/hep-ph/0703162) [HEP-PH]
22. H.N. Li, CERN Yellow Report CERN-2014-001, pp. 95–135. doi:[10.5170/CERN-2014-001.95](https://doi.org/10.5170/CERN-2014-001.95). arXiv:[1406.7689](https://arxiv.org/abs/1406.7689) [hep-ph]

23. W.F. Wang, H.N. Li, Phys. Lett. B **763**, 29 (2016). doi:10.1016/j.physletb.2016.10.026. arXiv:1609.04614 [hep-ph]
24. C.W. Bauer, D. Pirjol, I.W. Stewart, Phys. Rev. D **67**, 071502 (2003). doi:10.1103/PhysRevD.67.071502. arXiv:hep-ph/0211069
25. M. Beneke, T. Feldmann, Nucl. Phys. B **685**, 249 (2004). doi:10.1016/j.nuclphysb.2004.02.033. arXiv:hep-ph/0311335
26. C.W. Bauer, D. Pirjol, I.Z. Rothstein, I.W. Stewart, Phys. Rev. D **70**, 054015 (2004). doi:10.1103/PhysRevD.70.054015. arXiv:hep-ph/0401188
27. C.W. Bauer, I.Z. Rothstein, I.W. Stewart, Phys. Rev. D **74**, 034010 (2006). doi:10.1103/PhysRevD.74.034010. arXiv:hep-ph/0510241
28. T. Becher, A. Broggio, A. Ferroglia, Lect. Notes Phys. **896** (2015). doi:10.1007/978-3-319-14848-9. arXiv:1410.1892 [hep-ph]
29. S. Descotes-Genon, C.T. Sachrajda, Nucl. Phys. B **625**, 239 (2002). doi:10.1016/S0550-3213(02)00017-2. arXiv:hep-ph/0109260
30. M. Ciuchini, E. Franco, G. Martinelli, M. Pierini, L. Silvestrini, Phys. Lett. B **515**, 33 (2001). doi:10.1016/S0370-2693(01)00700-6. arXiv:hep-ph/0104126
31. M. Beneke, G. Buchalla, M. Neubert, C.T. Sachrajda, Phys. Rev. D **72**, 098501 (2005). doi:10.1103/PhysRevD.72.098501. arXiv:hep-ph/0411171
32. A.V. Manohar, I.W. Stewart, Phys. Rev. D **76**, 074002 (2007). doi:10.1103/PhysRevD.76.074002. arXiv:hep-ph/0605001
33. H.N. Li, S. Mishima, Phys. Rev. D **83**, 034023 (2011). doi:10.1103/PhysRevD.83.034023. arXiv:0901.1272 [hep-ph]
34. F. Feng, J.P. Ma, Q. Wang, arXiv:0901.2965 [hep-ph]
35. M. Beneke, G. Buchalla, M. Neubert, C.T. Sachrajda, Eur. Phys. J. C **61**, 439 (2009). doi:10.1140/epjc/s10052-009-1028-9. arXiv:0902.4446 [hep-ph]
36. T. Becher, G. Bell, Phys. Lett. B **713**, 41 (2012). doi:10.1016/j.physletb.2012.05.016. arXiv:1112.3907 [hep-ph]
37. M. Beneke, Nucl. Part. Phys. Proc. **261–262**, 311 (2015). doi:10.1016/j.nuclphysbps.2015.03.021. arXiv:1501.07374 [hep-ph]
38. B. Aubert et al., BABAR Collaboration, Phys. Rev. D **80**, 112001 (2009). doi:10.1103/PhysRevD.80.112001. arXiv:0905.3615 [hep-ex]
39. B. Aubert et al., BABAR Collaboration, Phys. Rev. D **78**, 012004 (2008). doi:10.1103/PhysRevD.78.012004. arXiv:0803.4451 [hep-ex]
40. J.P. Lees et al., BABAR Collaboration, Phys. Rev. D **83**, 112010 (2011). doi:10.1103/PhysRevD.83.112010. arXiv:1105.0125 [hep-ex]
41. J. P. Lees et al., [BABAR Collaboration], arXiv:1501.00705 [hep-ex]
42. J.P. Lees et al., [BABAR Collaboration], Phys. Rev. D **84**, 092007 (2011). doi:10.1103/PhysRevD.84.092007. arXiv:1109.0143 [hep-ex]
43. A. Garmash et al., [Belle Collaboration], Phys. Rev. Lett. **96**, 251803 (2006). doi:10.1103/PhysRevD.79.072004. arXiv:0811.3665 [hep-ex]
44. J. Dalseno et al., [Belle Collaboration], Phys. Rev. D **79**, 072004 (2009). doi:10.1103/PhysRevD.79.072004. arXiv:0811.3665 [hep-ex]
45. B. Bhattacharya, M. Gronau, J.L. Rosner, Phys. Lett. B **726**, 337 (2013). doi:10.1016/j.physletb.2013.08.062. arXiv:1306.2625 [hep-ph]
46. B. Bhattacharya, D. London, JHEP **1504**, 154 (2015). doi:10.1007/JHEP04(2015)154. arXiv:1503.00737 [hep-ph]
47. B. Bhattacharya, M. Gronau, M. Imbeault, D. London, J.L. Rosner, Phys. Rev. D **89**(7), 074043 (2014). doi:10.1103/PhysRevD.89.074043. arXiv:1402.2909 [hep-ph], and references therein
48. J.H. Alvarenga Nogueira et al., arXiv:1605.03889 [hep-ex]
49. K. Abe et al. [Belle Collaboration], arXiv:0708.1845 [hep-ex]
50. B. Aubert et al., [BaBar Collaboration], Phys. Rev. D **76**, 071101 (2007). doi:10.1103/PhysRevD.76.071101. arXiv:hep-ex/0702010
51. L.A. Pérez Pérez, Time-dependent amplitude analysis of $B^0 \rightarrow K_s \pi^+ \pi^-$ decays with the BABAR Experiment and constraints on the CKM matrix using the $B \rightarrow K^* \pi$ and $B \rightarrow \rho K$ modes
52. Y. Nir, H.R. Quinn, Phys. Rev. Lett. **67**, 541 (1991). doi:10.1103/PhysRevLett.67.541
53. M. Gronau, J. Zupan, Phys. Rev. D **71**, 074017 (2005). doi:10.1103/PhysRevD.71.074017. arXiv:hep-ph/0502139
54. F.J. Botella, J.P. Silva, Phys. Rev. D **71**, 094008 (2005). doi:10.1103/PhysRevD.71.094008. arXiv:hep-ph/0503136
55. M. Beneke, S. Jäger, Nucl. Phys. B **768**, 51 (2007). doi:10.1016/j.nuclphysb.2007.01.016. arXiv:hep-ph/0610322
56. G. Bell, V. Pilipp, Phys. Rev. D **80**, 054024 (2009). doi:10.1103/PhysRevD.80.054024. arXiv:0907.1016 [hep-ph]
57. G. Bell, M. Beneke, T. Huber, X.Q. Li, Phys. Lett. B **750**, 348 (2015). doi:10.1016/j.physletb.2015.09.037. arXiv:1507.03700 [hep-ph]
58. F.J. Botella, D. London, J.P. Silva, Phys. Rev. D **73**, 071501 (2006). doi:10.1103/PhysRevD.73.071501. arXiv:hep-ph/0602060
59. M. Gronau, D. London, Phys. Rev. Lett. **65**, 3381 (1990). doi:10.1103/PhysRevLett.65.3381
60. A.J. Buras, R. Fleischer, Eur. Phys. J. C **11**, 93 (1999). doi:10.1007/s100529900201, doi:10.1007/s100520050617. arXiv:hep-ph/9810260
61. M. Neubert, J.L. Rosner, Phys. Lett. B **441**, 403 (1998). doi:10.1016/S0370-2693(98)01194-0. arXiv:hep-ph/9808493
62. M. Neubert, J.L. Rosner, Phys. Rev. Lett. **81**, 5076 (1998). doi:10.1103/PhysRevLett.81.5076. arXiv:hep-ph/9809311
63. M. Gronau, Phys. Rev. Lett. **91**, 139101 (2003). doi:10.1103/PhysRevLett.91.139101. arXiv:hep-ph/0305144
64. M. Ciuchini, M. Pierini, L. Silvestrini, Phys. Rev. D **74**, 051301 (2006). doi:10.1103/PhysRevD.74.051301. arXiv:hep-ph/0601233
65. M. Gronau, D. Pirjol, A. Soni, J. Zupan, Phys. Rev. D **75**, 014002 (2007). doi:10.1103/PhysRevD.75.014002. arXiv:hep-ph/0608243
66. Y. Amhis et al., arXiv:1612.07233 [hep-ex]
67. J. Charles, S. Descotes-Genon, V. Niess, L. Vale Silva, arXiv:1611.04768 [hep-ph]
68. R. Aaij et al., [LHCb Collaboration], Phys. Rev. D **90**(11), 112004 (2014). doi:10.1103/PhysRevD.90.112004. arXiv:1408.5373 [hep-ex]
69. P. Urquijo, Nucl. Part. Phys. Proc. **263–264**, 15 (2015). doi:10.1016/j.nuclphysbps.2015.04.004. Belle II. <https://www.belle2.org/>
70. R. Aaij et al., [LHCb Collaboration], Phys. Rev. Lett. **111**, 101801 (2013). arXiv:1306.1246 [hep-ex]
71. LHCb-CONF-2012-023, July 6, 2012
72. LHCb-CONF-2012-026, July 11, 2012
73. B. Aubert et al., [BABAR Collaboration], Phys. Rev. D **79**, 072009 (2009). doi:10.1103/PhysRevD.79.072009. arXiv:0902.1708 [hep-ex]
74. I. Adachi et al., [Belle Collaboration], Phys. Rev. Lett. **108**, 171802 (2012). doi:10.1103/PhysRevLett.108.171802. arXiv:1201.4643 [hep-ex]
75. P. Ball, R. Zwicky, Phys. Rev. D **71**, 014029 (2005). doi:10.1103/PhysRevD.71.014029. arXiv:hep-ph/0412079
76. A. Bharucha, D.M. Straub, R. Zwicky, JHEP **1608**, 098 (2016). doi:10.1007/JHEP08(2016)098. arXiv:1503.05534 [hep-ph]
77. V.M. Braun, D.Y. Ivanov, G.P. Korchemsky, Phys. Rev. D **69**, 034014 (2004). doi:10.1103/PhysRevD.69.034014. arXiv:hep-ph/0309330
78. S. Aoki et al., Eur. Phys. J. C **77**(2), 112 (2017). doi:10.1140/epjc/s10052-016-4509-7. arXiv:1607.00299 [hep-lat]

79. G. Bell, talk given at the workshop *Future Challenges in Non-Leptonic B Decays: Theory and Experiment*, Bad Honnef (Germany), 10–12 February 2016. <https://indico.cern.ch/event/458285/>
80. G. Bell, Nucl. Phys. B **795**, 1 (2008). doi:[10.1016/j.nuclphysb.2007.09.006](https://doi.org/10.1016/j.nuclphysb.2007.09.006). arXiv:[0705.3127](https://arxiv.org/abs/0705.3127) [hep-ph]
81. G. Bell, Nucl. Phys. B **822**, 172 (2009). doi:[10.1016/j.nuclphysb.2009.07.012](https://doi.org/10.1016/j.nuclphysb.2009.07.012). arXiv:[0902.1915](https://arxiv.org/abs/0902.1915) [hep-ph]
82. M. Beneke, T. Huber, X.Q. Li, Nucl. Phys. B **832**, 109 (2010). doi:[10.1016/j.nuclphysb.2010.02.002](https://doi.org/10.1016/j.nuclphysb.2010.02.002). arXiv:[0911.3655](https://arxiv.org/abs/0911.3655) [hep-ph]